

Edge states in super honeycomb structures with \mathcal{PT} symmetric deformations

Ying Cao*, Yi Zhu †

May 17, 2024

Abstract

The existence of edge states is one of the most vital properties of topological insulators. Although tremendous success has been accomplished in describing and explaining edge states associated with \mathcal{PT} symmetry breaking, little work has been done on \mathcal{PT} symmetry preserving cases. Two-dimensional Schrödinger operators with super honeycomb lattice potentials always have double Dirac cones at the Γ point – the zero momentum point on their energy bands due to C_6 symmetry, \mathcal{PT} symmetry, and the “folding” symmetry – caused by an additional translation symmetry. There are two topologically different ways to deform such a system by \mathcal{PT} symmetry preserving but folding symmetry breaking perturbations. Interestingly, there exist two gapped edge states on the interface between such two kinds of perturbed materials. In this paper, we illustrate the existence of such \mathcal{PT} preserving edge states rigorously for the first time. We use a domain wall modulated Schrödinger operator to model the phenomenon under small perturbations and rigorously prove the existence of two gapped edge states. We also provide a brief interpretation from the point of view of “topology” by the parities of degenerate bulk modes. Our work thoroughly explains the existence of “helical” like edge states in super honeycomb configurations and lays a foundation for the descriptions of topologies of such systems.

Keywords: super honeycomb lattice potentials; edge states; \mathcal{PT} symmetry; Schrödinger operator.

AMS Subject Classification: 35C20, 35P99, 35Q40, 35Q60

1 Introduction and notations

1.1 Introduction

The existence of interface conducting states is one of the most significant properties of topological insulators [18, 20]. It originates in certain energy gaps caused by symmetry breaking in

*Yau Mathematical Sciences Center, Tsinghua University, Beijing, 100084, China (caoy20@mails.tsinghua.edu.cn).

†Yau Mathematical Sciences Center, Tsinghua University, Beijing, 100084, China, and Beijing Institute of Mathematical Sciences and Applications, Beijing, 101408, China (yizhu@tsinghua.edu.cn).

the bulk. In the past two decades, there have been many efforts made to reveal the underlying mechanism of interface conducting states, mainly on the edge states caused by \mathcal{PT} symmetry breaking [14, 13, 11, 19]. However, physicists also find edge states in two-dimensional \mathcal{PT} symmetric materials [29]. In this paper, we model such phenomena by analyzing the spectral properties of a domain wall modulated Schrödinger operator.

One of the typical lattices whose deformed bulk has interface conducting states is the honeycomb lattice. The honeycomb lattice structure possesses single Dirac cones at K and K' points and chiral edge states after time-reversal symmetry breaking [1, 14, 13, 9, 11]. The most famous paradigm is graphene, a two-dimensional topological material [18]. Around 2015, a new way to deform the honeycomb lattice has been reported [29, 30, 31]. They considered the lattice in a supercell so that it has folding symmetry - caused by smaller periods than the supercell lattice. We call it a super honeycomb lattice in our previous work [8]. This new highly symmetric structure has fourfold degeneracy and a double Dirac cone at the Γ point. Deforming the super honeycomb lattice in two different directions makes the energy bands open a gap with different topologies near the Γ point [8, 22]. Physicists found a pair of gapped pseudospin edge states when connecting such two types of deformed materials, which are analogs of the helical edge states [24]. The propagation of electromagnetic waves with frequencies between these two edge states is well confined near the interface [7, 26]. Despite the broad applications of this phenomenon, it is rarely studied rigorously. Motivated by this, we consider edge operators interpolating between two kinds of perturbed operators across a rational edge and try to establish the existence of two gapped edge states by rigorous analysis.

Many models are used to develop analysis on edge states. Ammari and his collaborators studied the related mechanism on the subwavelength scale by considering Helmholtz problems [2, 3]. Bal and his collaborators have analyzed properties and topological descriptions of edge states in Dirac operators [4, 5]. Also, some numerical methods are introduced to associated problems [16, 17].

Among all the models, the one particle non-relativistic Schrödinger equation is one of the most effective models in illustrating edge conducting states [13, 21, 10, 11, 17]. Fefferman and Weinstein have laid solid foundations of rigorous analysis on such equations in both \mathcal{P} and \mathcal{T} breaking case [14, 12, 13]. In this paper, we consider the following two-dimensional Schrödinger operator:

$$\mathcal{H}_{edge}^\delta = -\Delta + V(\mathbf{x}) + \delta\eta(\delta\mathbf{l}_2 \cdot \mathbf{x})W(\mathbf{x}),$$

with $V(\mathbf{x})$ a super honeycomb lattice potential, $\eta(\zeta)$ a domain function, and $W(\mathbf{x})$ a \mathcal{PT} symmetry preserving perturbation; see section 2.3. The limiting perturbed bulk operators on two sides:

$$\mathcal{H}_\pm^\delta = -\Delta + V(\mathbf{x}) \pm \delta W(\mathbf{x})$$

are \mathcal{PT} symmetric, but the folding symmetry is missing. Different from the analysis of \mathcal{P} or \mathcal{T} breaking bulk operators [13, 21, 11], we have to deal with the double Dirac cone [8], or two tangent single Dirac cones on the bands of the unperturbed operator $\mathcal{H}_V = -\Delta + V(\mathbf{x})$, where a nontrivial second-order degeneracy is hidden; see section 3 and section 6.2. This means that only in higher-order terms can we clearly see the interaction between the four

branches when discussing edge states. Such behavior is deeply rooted in the \mathcal{PT} symmetry preserving property. In the time-reversal symmetry breaking case, a one-dimensional Dirac operator can be obtained as the effective model by asymptotic expansions. An edge state with energy near the Dirac point can be derived from its exponentially decaying zero-energy states [21, 10, 11]. However, when it comes to the time reversal symmetric case, there are a pair of paralleling Dirac operators and therefore, two indistinguishable zero-energy states. Thus, the energy gap between two edge states is of higher order and deserves precise description; see section 4.

Another exciting perspective of understanding the edge states is the interplay between the symmetries and topology. Similar to how the Chern numbers characterize the topology of quantum materials, some topological indices are introduced to characterize the topology of bulk and edge Hamiltonians and the bulk-edge correspondence [23, 25]. There exist results on some one-dimensional models [27, 28] and higher-dimensional Dirac operators [4, 5, 6]. Different from a quantity of the whole band, in this paper, we provide a topological view concentrated on the Γ point by analyzing the parities of the eigenstates of limiting bulk operators $\mathcal{H}_{\pm}^{\delta}$ on two sides of the edge, which connects the symmetries and the topology more explicitly; see section 6.1.

This paper is organized as follows. Section 2 introduces the problem and our model – the domain wall modulated edge operator. Results on super honeycomb lattice potentials and double Dirac cones are briefly reviewed in this section. Section 3 establishes the approximations of the eigenstates near the double Dirac cone. Such near-energy approximations play essential roles in calculating the two gapped edge states asymptotically and rigorously proving their existence. The following three sections focus on the main conclusions obtained from our model. Section 4 calculates two edge states explicitly by multiscale expansions. Section 5 proves the existence of two gapped edge states rigorously. Section 6 is about some physical interpretations. Section 6.1 provides a topological perspective by parties; section 6.2 addresses the relations between the bifurcations and the \mathcal{PT} symmetry preserving property; and section 6.3 gives numerical simulation of a typical example.

1.2 Notations

- $\mathbf{U} = \mathbb{Z}\mathbf{u}_1 \oplus \mathbb{Z}\mathbf{u}_2$ denotes the parallelogram lattice in \mathbb{R}^2 expanding by \mathbf{u}_1 and \mathbf{u}_2 . $\Omega = \{\mathbf{u} = c_1\mathbf{u}_1 + c_2\mathbf{u}_2 : c_1, c_2 \in (-1/2, 1/2)\}$ denotes its fundamental cell. $\mathbf{U}^* = \mathbb{Z}\mathbf{k}_1 \oplus \mathbb{Z}\mathbf{k}_2$ denotes its dual lattice with $\mathbf{k}_l \cdot \mathbf{u}_j = 2\pi\delta_{l,j}$. $\Omega^* = \mathbb{R}^2/\mathbf{U}^*$ is the fundamental cell of its dual lattice and is called the Brillouin Zone.
- $\mathbf{w}_1 = a_1\mathbf{u}_1 + b_1\mathbf{u}_2$; $\mathbf{w}_2 = a_2\mathbf{u}_1 + b_2\mathbf{u}_2$. a_1, b_1, a_2, b_2 are integers and $a_1b_2 - a_2b_1 = 1$. $\mathbf{l}_1 = b_2\mathbf{k}_1 - a_2\mathbf{k}_2$ and $\mathbf{l}_2 = -b_1\mathbf{k}_1 + a_1\mathbf{k}_2$ satisfy $\mathbf{w}_l \cdot \mathbf{l}_j = 2\pi\delta_{l,j}$. $\tilde{\mathbf{l}}_1 = \mathbf{l}_1 - \frac{\mathbf{l}_1 \cdot \mathbf{l}_2}{\|\mathbf{l}_2\|^2}\mathbf{l}_2$ is orthogonal to \mathbf{l}_2 and satisfies $\tilde{\mathbf{l}}_1 \cdot \mathbf{w}_1 = 2\pi$.
- $\Omega_e = \{\mathbf{u} = c_1\mathbf{w}_1 + c_2\mathbf{w}_2 : c_1 \in (-1/2, 1/2), c_2 \in \mathbb{R}\}$.
- There are three different inner products:

1. $\langle f(\mathbf{x}), g(\mathbf{x}) \rangle_{L^2(\Omega)} = \int_{\Omega} \overline{f(\mathbf{x})} g(\mathbf{x}) d\mathbf{x};$
2. $\langle f(\mathbf{x}), g(\mathbf{x}) \rangle_{L^2(\Omega_e)} = \int_{\Omega_e} \overline{f(\mathbf{x})} g(\mathbf{x}) d\mathbf{x};$
3. $\langle f(\zeta), g(\zeta) \rangle_{L^2(\mathbb{R})} = \int_{\mathbb{R}} \overline{f(\zeta)} g(\zeta) d\zeta.$

- There are two particular function spaces often used:

$$\chi = \{f \in L^2_{loc}(\mathbb{R}^2) : f(\mathbf{x} + \mathbf{u}_l) = f(\mathbf{x}), l = 1, 2\};$$

$$\chi_e = \{f \in L^2_{loc}(\mathbb{R}^2) : f(\mathbf{x} + \mathbf{w}_1) = f(\mathbf{x}), \int_{\Omega_e} |f(\mathbf{x})|^2 d\mathbf{x} < \infty\}.$$

- Pauli matrices:

$$\sigma_1 = \begin{pmatrix} 0 & 1 \\ 1 & 0 \end{pmatrix}; \quad \sigma_2 = \begin{pmatrix} 0 & -i \\ i & 0 \end{pmatrix}; \quad \sigma_3 = \begin{pmatrix} 1 & 0 \\ 0 & -1 \end{pmatrix}.$$

2 Bulk and edge operators

The original bulk Hamiltonians should have C_6 , \mathcal{PT} , and folding symmetries. We have studied such Schrödinger operators in the form of $\mathcal{H}_V = -\Delta + V(\mathbf{x})$, where $V(\mathbf{x})$ is a super honeycomb lattice potential as in Definition 2.2. The perturbed bulk operator is $\mathcal{H}^\delta = -\Delta + V(\mathbf{x}) + \delta W(\mathbf{x})$, where $W(\mathbf{x})$ preserves C_6 and \mathcal{PT} symmetries but destroys the folding symmetry [8]. There should be two gapped edge states when gluing two kinds of perturbed bulk operators along certain edges, as shown in Figure 1. In this paper, we talk about an asymptotic model - the domain wall modulated Schrödinger operator:

$$\mathcal{H}_{edge}^\delta = -\Delta + V(\mathbf{x}) + \delta\eta(\delta\mathbf{l}_2 \cdot \mathbf{x})W(\mathbf{x}),$$

where $\eta(\zeta)$ is a domain wall function as in Definition 2.8. $\mathcal{H}_{edge}^\delta$ is a slow interpolation between $\mathcal{H}_\pm^\delta = -\Delta + V(\mathbf{x}) \pm \delta W(\mathbf{x})$ across a rational edge $\mathbb{R}\mathbf{w}_1$. This section briefly reviews bulk operators, including their symmetries and the degeneracy on their bands at the Γ point, and introduces the edge operator.

2.1 Super honeycomb lattice potentials and the folding symmetry

In this subsection, we review the symmetries of super honeycomb lattice potentials. It originates in viewing the honeycomb lattice in a supercell. Thus, the super honeycomb lattice possesses a folding symmetry, which results in fourfold degeneracy at the Γ point on energy bands.

Fefferman and Weinstein have summarized the structures of the honeycomb lattice in their paper [14]. It is such a periodic structure in \mathbb{R}^2 :

- $\frac{2}{3}\pi$ -rotation symmetric;
- \mathcal{PT} (parity and time reversal) symmetric.

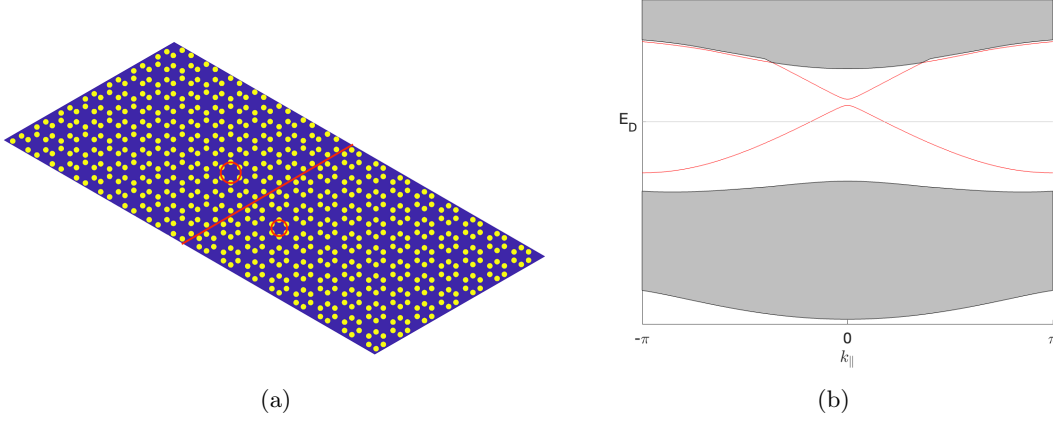


Figure 1: Numerical simulations of edge states curves of a limiting domain wall model. (a) the figure of the piecewise constant domain wall potential. On one side of the edge, the hexagons of the super honeycomb lattice are shrunk, and on the other side, they are expanded. (b) the figure of the edge states energy curves along $k_{\parallel} \tilde{l}_1$. E_D is the Dirac point's energy. The parts of two red curves near the Γ point correspond to two edge states.

The corresponding transformations in $L^2_{loc}(\mathbb{R}^2)$ are:

- $\frac{2}{3}\pi$ rotation operator \mathcal{R} : $\mathcal{R}[f](\mathbf{x}) = f(R^*\mathbf{x})$ with $R^* = \begin{pmatrix} -\frac{1}{2} & -\frac{\sqrt{3}}{2} \\ \frac{\sqrt{3}}{2} & -\frac{1}{2} \end{pmatrix}$;
- reflection operator \mathcal{P} : $\mathcal{P}[f](\mathbf{x}) = f(-\mathbf{x})$;
- time reversal operator \mathcal{T} : $\mathcal{T}[f](\mathbf{x}) = \overline{f(\mathbf{x})}$.

Definition 2.1 (Honeycomb lattice potentials) $V(\mathbf{x}) \in C^\infty(\mathbb{R}^2)$ is called a honeycomb lattice potential, if

1. $V(\mathbf{x})$ is doubly periodic with periods \mathbf{u}_1 and \mathbf{u}_2 , where $\mathbf{u}_2 = -R^*\mathbf{u}_1$;
2. $\mathcal{R}[V](\mathbf{x}) = V(\mathbf{x})$;
3. $\mathcal{P}[V](\mathbf{x}) = V(\mathbf{x})$ and $\mathcal{T}[V](\mathbf{x}) = V(\mathbf{x})$.

Consider the parallelogram lattice $\mathbf{U} = \mathbb{Z}\mathbf{u}_1 \oplus \mathbb{Z}\mathbf{u}_2$. The corresponding unit cell is

$$\Omega = \{\mathbf{u} = c_1\mathbf{u}_1 + c_2\mathbf{u}_2, \quad c_1, c_2 \in (-1/2, 1/2)\}. \quad (2.1)$$

Denote its dual lattice and dual unit cell $\mathbf{U}^* = \mathbb{Z}\mathbf{k}_1 \oplus \mathbb{Z}\mathbf{k}_2$ and $\Omega^* = \mathbb{R}^2/\mathbf{U}^*$, where \mathbf{k}_j satisfies $\mathbf{u}_i \cdot \mathbf{k}_j = 2\pi\delta_{i,j}$.

The relation and differences between honeycomb lattice and super honeycomb lattice are shown explicitly in Figure 2. Note that the parallelogram lattice discussed above and the hexagonal lattice in the pictures are equivalent. Compared with the honeycomb lattice

potentials, the super honeycomb lattice potential obscures smaller periods and, therefore, a folding symmetry. Namely, the smaller periods are

$$\mathbf{v}_1 = \frac{1}{3}(2\mathbf{u}_1 - \mathbf{u}_2), \quad \mathbf{v}_2 = \frac{1}{3}(\mathbf{u}_1 + \mathbf{u}_2). \quad (2.2)$$

For simplicity, denote translation operators: $\mathcal{V}_l[f](\mathbf{x}) = f(x + \mathbf{v}_l)$. Let \mathbf{q}_j be the dual vectors of \mathbf{v}_l , i.e., $\mathbf{q}_j \cdot \mathbf{v}_l = 2\pi\delta_{j,l}$.

The super honeycomb lattice potential is defined below.

Definition 2.2 (Super honeycomb lattice potentials) *A honeycomb lattice potential $V(\mathbf{x}) \in C^\infty(\mathbb{R}^2)$ is called a super honeycomb lattice potential if*

4. $V(\mathbf{x})$ is \mathbf{v}_1 and \mathbf{v}_2 periodic, where \mathbf{v}_1 and \mathbf{v}_2 are as in (2.2) and the following condition holds:

$$\frac{1}{|\Omega|} \int_{\Omega} e^{-i\mathbf{q}_1 \cdot \mathbf{y}} V(\mathbf{y}) d\mathbf{y} \neq 0. \quad (2.3)$$

Remark 2.3 *The condition (2.3) guarantees that the lowest Fourier element of $V(\mathbf{x})$ does not vanish, which prevents $V(\mathbf{x})$ from being a constant or possessing smaller periods.*

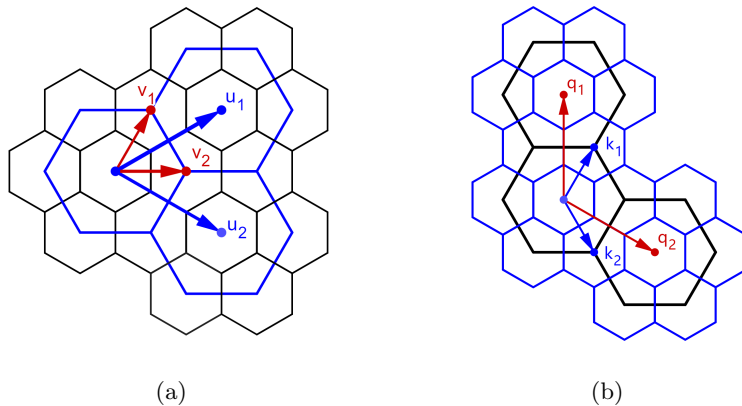


Figure 2: (a) The lattice, and (b) the dual lattice. The blue lattice corresponds to a honeycomb lattice, with periods \mathbf{u}_1 and \mathbf{u}_2 and dual periods \mathbf{k}_1 and \mathbf{k}_2 . The black lattice corresponds to the associated super honeycomb lattice, with periods \mathbf{v}_1 and \mathbf{v}_2 and dual periods \mathbf{q}_1 and \mathbf{q}_2 .

2.2 Bulk operators

The bulk operators $\mathcal{H}_\pm^\delta = -\Delta + V(\mathbf{x}) \pm \delta W(\mathbf{x})$ on two sides of the edge are deformed from the highly symmetric operator $\mathcal{H}_V = -\Delta + V(\mathbf{x})$, where $V(\mathbf{x})$ is a super honeycomb lattice potential. In this subsection, we give two conclusions about \mathcal{H}_V and $\mathcal{H}^\delta = -\Delta + V(\mathbf{x}) + \delta W(\mathbf{x})$ [8].

Generally, for a \mathbf{u}_1 and \mathbf{u}_2 doubly periodic elliptic operator \mathcal{H} , by Floquet-Bloch theorem, its spectrum can be decomposed into momentum space Ω^* :

$$\sigma_{L^2(\mathbb{R}^2)}(\mathcal{H}) = \bigcup_{\mathbf{k} \in \Omega^*} \sigma_{L_{\mathbf{k}}^2(\mathbb{R}^2/\mathbf{U})}(\mathcal{H}|_{L_{\mathbf{k}}^2(\mathbb{R}^2/\mathbf{U})}).$$

Here the \mathbf{k} -momentum function space is the Hilbert space

$$L_{\mathbf{k}}^2(\mathbb{R}^2/\mathbf{U}) = \{f \in L_{loc}^2(\mathbb{R}^2) : f(\mathbf{x} + \mathbf{u}) = e^{i\mathbf{k} \cdot \mathbf{u}} f(\mathbf{x}), \mathbf{x} \in \mathbb{R}^2, \mathbf{u} \in \mathbf{U}; f(\mathbf{x}) \in L^2(\Omega)\}$$

equipped with the inner product:

$$\langle f(\mathbf{x}), g(\mathbf{x}) \rangle_{L^2(\Omega)} = \int_{\Omega} \overline{f(\mathbf{x})} g(\mathbf{x}) d\mathbf{x}. \quad (2.4)$$

For our bulk operators, $\sigma_{L_{\mathbf{k}}^2(\mathbb{R}^2/\mathbf{U})}(\mathcal{H}|_{L_{\mathbf{k}}^2(\mathbb{R}^2/\mathbf{U})})$ is a lower bounded discrete set:

$$E_1(\mathbf{k}) \leq E_2(\mathbf{k}) \leq E_3(\mathbf{k}) \leq \dots \quad (2.5)$$

$\mathcal{S}_n = \{(\mathbf{k}, E_n(\mathbf{k})) : \mathbf{k} \in \Omega^*\}$ is the n^{th} energy surface of \mathcal{H} . Dirac cone describes the phenomenon of conical touch between energy surfaces. It is a kind of degeneracy and singularity on energy surfaces.

The first conclusion is that \mathcal{H}_V has fourfold degeneracy at the Γ point and a double Dirac cone for general super honeycomb lattice potential $V(\mathbf{x})$ due to the symmetry. The key is that the space of \mathbf{u}_1 and \mathbf{u}_2 periodic functions $\chi = L_{\mathbf{0}}^2(\mathbb{R}^2/\mathbf{U})$ has the decomposition:

$$\chi = \bigoplus_{\xi_1, \xi_2=1, \tau, \bar{\tau}} \chi_{\xi_1, \xi_2}, \quad \tau = e^{\frac{2}{3}\pi i}. \quad (2.6)$$

χ_{ξ_1, ξ_2} is the intersection of the characteristic subspace of \mathcal{V}_1 with eigenvalue ξ_1 and the characteristic subspace of \mathcal{R} with eigenvalue ξ_2 . Because any super honeycomb lattice potential $V(\mathbf{x})$ is in $\chi_{1,1}$, \mathcal{H}_V has the rotation and folding symmetries. Thus, each χ_{ξ_1, ξ_2} is an invariant subspace of \mathcal{H}_V . The following theorem shows the existence of fourfold degeneracy and its relationship with the above function space decomposition.

Theorem 2.4 (Fourfold degeneracy at the Γ point) *The following is true for energy surfaces of $\mathcal{H}^{(\epsilon)} = -\Delta + \epsilon V(\mathbf{x})$ with $V(\mathbf{x})$ a super honeycomb lattice potential for all $\epsilon \in \mathbb{R} \setminus A$, where A is a discrete subset of \mathbb{R} :*

1. *there exists $n_* \in \mathbb{N}$ and $E_D \in \mathbb{R}$ such that $\{\mathcal{S}_{n_*+j}\}_{j=1,2,3,4}$ intersect at the Γ point:*

$$E_{n_*}(\mathbf{0}) < E_D = E_{n_*+1}(\mathbf{0}) = E_{n_*+2}(\mathbf{0}) = E_{n_*+3}(\mathbf{0}) = E_{n_*+4}(\mathbf{0}) < E_{n_*+5}(\mathbf{0}); \quad (2.7)$$

2. *there exists $\phi_1(\mathbf{x}) \in \chi_{\tau, \tau}$ normalized, such that*

$$\text{Ker}(\mathcal{H}^{(\epsilon)} - E_D) = \text{Span} \{\phi_1(\mathbf{x}), \phi_2(\mathbf{x}), \phi_3(\mathbf{x}), \phi_4(\mathbf{x})\};$$

and the four eigenstates satisfy:

$$\begin{aligned} \phi_1(\mathbf{x}) &\in \chi_{\tau, \tau}, & \phi_2(\mathbf{x}) &= \overline{\phi_1(-\mathbf{x})} \in \chi_{\tau, \bar{\tau}}, \\ \phi_3(\mathbf{x}) &= \phi_1(-\mathbf{x}) \in \chi_{\bar{\tau}, \tau}, & \phi_4(\mathbf{x}) &= \overline{\phi_1(\mathbf{x})} \in \chi_{\bar{\tau}, \bar{\tau}}. \end{aligned} \quad (2.8)$$

Equation (2.7) indicates the existence of a fourfold degeneracy at the Γ point. (2.8) provides insight into the four eigenfunctions corresponding to this degeneracy, revealing that they can be related through symmetries. We will give the result of the double Dirac cone later after we calculate the second-order bifurcation terms; see section 3.1.

The second conclusion is that the energy surfaces of \mathcal{H}^δ open a gap of order $O(\delta)$ at the Γ point when $W(\mathbf{x})$ is a folding symmetry breaking potential as in the following definition.

Definition 2.5 (Folding symmetry breaking potentials) *A folding symmetry breaking potential $W(\mathbf{x})$ is a function in $C^\infty(\mathbb{R}^2)$ satisfying:*

- \mathcal{PT} symmetry preserving : $W(\mathbf{x})$ is a honeycomb lattice potential;
- folding symmetry breaking: $W(\mathbf{x}) \in \chi_{\tau,1} \oplus \chi_{\bar{\tau},1}$, which means $W(\mathbf{x})$ is orthogonal to the space of super honeycomb lattice potentials so that it is “purely” folding symmetry breaking.

The second conclusion is stated precisely as follows.

Theorem 2.6 (Local gap under folding symmetry breaking perturbations) *Let $\mathcal{H}_V = -\Delta + V(\mathbf{x})$ be an operator possessing a fourfold degeneracy at the Γ point as in Theorem 2.4. Assume that $W(\mathbf{x})$ is a folding symmetry breaking potential as above in Definition 2.5 and satisfies the non-degeneracy condition:*

$$c_\sharp = \langle \phi_1(\mathbf{x}), W(\mathbf{x})\phi_1(-\mathbf{x}) \rangle_{L^2(\Omega)} \neq 0. \quad (2.9)$$

Then the energy surfaces $\{\mathcal{S}_{n_+j}\}_{j=1,2,3,4}$ of perturbed operator $\mathcal{H}^\delta = -\Delta + V(\mathbf{x}) + \delta W(\mathbf{x})$ will open a gap of $O(|\delta|)$ near the Γ point for δ sufficiently small.*

Remark 2.7 *The c_\sharp is real and stays invariant under phase transformation [8]. Nonzero c_\sharp guarantees that the gap is of order $O(\delta)$ exactly.*

2.3 Domain wall modulated edge operator

In this paper, we consider two kinds of bulks $\mathcal{H}_\pm^\delta = -\Delta + V(\mathbf{x}) \pm \delta W(\mathbf{x})$ connected along a rational edge $\mathbb{R}\mathbf{w}_1$. Here $\mathbf{w}_1 = a_1\mathbf{u}_1 + b_1\mathbf{u}_2$, where a_1 and b_1 are relatively prime integers. Then there exist relatively prime integers a_2, b_2 such that $a_1b_2 - a_2b_1 = 1$. Let $\mathbf{w}_2 = a_2\mathbf{u}_1 + b_2\mathbf{u}_2$. Take $\mathbf{l}_1 = b_2\mathbf{k}_1 - a_2\mathbf{k}_2$ and $\mathbf{l}_2 = -b_1\mathbf{k}_1 + a_1\mathbf{k}_2$. Then $\mathbf{w}_j \cdot \mathbf{l}_l = 2\pi\delta_{j,l}$. Note that \mathbf{w}_1 and \mathbf{w}_2 expands a cell equivalent to Ω and \mathbf{l}_1 and \mathbf{l}_2 expands a cell equivalent to Ω^* . Let Ω_e denote such an area around the edge:

$$\Omega_e = \{\mathbf{x} \in \mathbb{R}^2 \mid \mathbf{x} = p\mathbf{w}_1 + q\mathbf{w}_2, p \in (-1/2, 1/2), q \in \mathbb{R}\}.$$

For the rational edge $\mathbb{R}\mathbf{w}_1$, we use the following asymptotic domain wall modulated operator:

$$\mathcal{H}_{edge}^\delta = -\Delta + V(\mathbf{x}) + \delta\eta(\delta\mathbf{l}_2 \cdot \mathbf{x})W(\mathbf{x}). \quad (2.10)$$

The limiting bulk operators \mathcal{H}_\pm^δ have been introduced in the last subsection. The function $\eta(\delta\mathbf{l}_2 \cdot \mathbf{x})$ is the domain wall modulation function. It is flat along the edge direction \mathbf{w}_1 and varies slowly in the direction \mathbf{w}_2 . $\zeta = \delta\mathbf{l}_2 \cdot \mathbf{x}$ is called the slow variable. The rigorous definition of a domain wall function $\eta(\zeta)$ is below.

Definition 2.8 (Domain wall functions) *A smooth function $\eta(\zeta) \in C^\infty(\mathbb{R})$ is called a domain wall function if $\eta(\zeta)$ tends to ± 1 when $\zeta \rightarrow \pm\infty$ and $\eta(0) = 0$.*

Similar to that in bulk case, we have:

$$\sigma_{L^2(\mathbb{R}^2)}(\mathcal{H}_{edge}^\delta) = \bigcup_{k_\parallel \in [-\pi, \pi)} \sigma_{L^2_{k_\parallel}(\mathbb{R}^2/\mathbb{Z}\mathbf{w}_1)}(\mathcal{H}_{edge}^\delta|_{L^2_{k_\parallel}(\mathbb{R}^2/\mathbb{Z}\mathbf{w}_1)}).$$

Here the function space is one-dimensional quasi-periodic:

$$L^2_{k_\parallel}(\mathbb{R}^2/\mathbb{Z}\mathbf{w}_1) = \{f \in L^2_{loc}(\mathbb{R}^2) : f(\mathbf{x} + \mathbf{w}_1) = e^{ik_\parallel} f(\mathbf{x}), \mathbf{x} \in \mathbb{R}^2; f(\mathbf{x}) \in L^2(\Omega_e)\}.$$

The inner product on $L^2_{k_\parallel}(\mathbb{R}^2/\mathbb{Z}\mathbf{w}_1)$ is :

$$\langle f, g \rangle_{L^2(\Omega_e)} = \int_{\Omega_e} \overline{f(\mathbf{x})} g(\mathbf{x}) d\mathbf{x}. \quad (2.11)$$

We summarize our asymptotic model in the following definition.

Definition 2.9 (Folding symmetry breaking domain wall modulated edge operators) $\mathcal{H}_{edge}^\delta = -\Delta + V(\mathbf{x}) + \delta\eta(\delta\mathbf{l}_2 \cdot \mathbf{x})W(\mathbf{x})$ is called a folding symmetry breaking domain wall modulated edge operator if it is constructed as follows.

- The unperturbed bulk operator has a fourfold degeneracy: $\mathcal{H}_V = -\Delta + V(\mathbf{x})$ with $V(\mathbf{x})$ a super honeycomb lattice potential is an operator possessing fourfold degeneracy $(\mathbf{0}, E_D)$ at the Γ point on $(n_* + 1)^{th}$ to $(n_* + 4)^{th}$ bands as (2.7) and (2.8) in Theorem 2.4.
- For $j = 1, 2, 3, 4$, the energy band $E_{n_*+j}(\mathbf{k})$ of \mathcal{H}_V satisfies the non-fold condition:

$$E_{n_*+j}(\lambda\mathbf{l}_2) = E_D \Leftrightarrow \text{there exists } m, n \in \mathbb{Z}, \text{ such that } \lambda\mathbf{l}_2 = m\mathbf{k}_1 + n\mathbf{k}_2. \quad (2.12)$$

- The folding symmetry is broken but the \mathcal{PT} symmetry is preserved: $W(\mathbf{x})$ is a folding symmetry breaking potential as in Definition 2.5.
- The domain wall is rational: $\eta(\zeta)$ is a domain wall function as in Definition 2.8 and $\mathbf{l}_2 = -b_1\mathbf{k}_1 + a_1\mathbf{k}_2$ for some co-prime b_1 and a_1 .

Remark 2.10 *By the continuity of the spectral band, the condition (2.12) means that E_D are the maximum or minimum of the lower or upper bands of the double Dirac cone along the \mathbf{l}_2 direction. This is a typical case when the four intersecting bands can open an energy gap along the \mathbf{l}_2 direction across the Γ point under small folding symmetry breaking perturbations.*

Our aim is to solve the following eigenvalue problem near $k_\parallel = 0$:

$$\mathcal{H}_{edge}^\delta \psi(\mathbf{x}, k_\parallel) = \mathcal{E}(k_\parallel) \psi(\mathbf{x}, k_\parallel), \quad \psi(\mathbf{x}, k_\parallel) \in L^2_{k_\parallel}(\mathbb{R}^2/\mathbb{Z}\mathbf{w}_1). \quad (2.13)$$

The following sections contribute to proving the existence of two gapped edge states near $k_\parallel = 0$ and characterizing these two edge states precisely.

3 Near-energy approximation

This section focuses on detailed information on the near-energy approximations – the approximations of energies and eigenstates of \mathcal{H}_V with energy near E_D , which helps to approximate the near-energy components when proving the existence of two gapped edge states in the following sections. More accurate results than the previous ones are needed because the first-order bifurcation matrix is still degenerate [8]. For the four branches of energy surfaces intersecting at the Γ point, the upper two do not separate at order $O(\|\mathbf{k}\|)$, nor do the lower two. The second-order bifurcation matrix is calculated in this section so that the near-energy approximation along the direction \mathbf{l}_2 can be given precisely.

3.1 Order $O(\|\mathbf{k}\|^2)$ bifurcation matrix

This subsection discusses the bifurcation matrices for any \mathbf{k} sufficiently small to estimate the near-energy eigenstates.

The eigenvalue problem of \mathcal{H}_V on $L_{\mathbf{k}}^2(\mathbb{R}^2/\mathbf{U})$:

$$\begin{aligned}\mathcal{H}_V\phi(\mathbf{x};\mathbf{k}) &= E(\mathbf{k})\phi(\mathbf{x};\mathbf{k}), \\ \phi(\mathbf{x};\mathbf{k}) &= e^{i\mathbf{k}\cdot\mathbf{x}}p(\mathbf{x}), \quad p(\mathbf{x}) \in \chi;\end{aligned}$$

is equivalent to

$$\mathcal{H}_V(\mathbf{k})p(\mathbf{x};\mathbf{k}) = E(\mathbf{k})p(\mathbf{x};\mathbf{k}), \quad p(\mathbf{x}) \in \chi,$$

where $\mathcal{H}_V(\mathbf{k}) = -(\nabla + i\mathbf{k})^2 + V(\mathbf{x})$.

We only consider the near-energy solution:

$$E(\mathbf{k}) = E_D + \mu, \quad p(\mathbf{x};\mathbf{k}) = \Phi(\mathbf{x})^T \mathbf{P}(\mathbf{k}) + \psi(\mathbf{x};\mathbf{k}).$$

where $\mathbf{P}(\mathbf{k}) = (p_1(\mathbf{k}), p_2(\mathbf{k}), p_3(\mathbf{k}), p_4(\mathbf{k}))^T$, $\psi(\mathbf{x};\mathbf{k}) \in \text{Ker}(\mathcal{H}_V - E_D)^\perp$, the corrector μ and $\psi(\mathbf{x};\mathbf{k})$ are small, and

$$\Phi(\mathbf{x}) = (\phi_1(\mathbf{x}), \phi_2(\mathbf{x}), \phi_3(\mathbf{x}), \phi_4(\mathbf{x}))^T. \quad (3.1)$$

Here $\{\phi_j(\mathbf{x})\}_j$ span $\text{Ker}(\mathcal{H}_V - E_D)$ as in (2.8). Substitute these into the eigenvalue problem and rearrange it into:

$$(\mathcal{H}_V - E_D)\psi(\mathbf{x};\mathbf{k}) = (\mu + 2i\mathbf{k} \cdot \nabla - \|\mathbf{k}\|^2)(\Phi(\mathbf{x})^T \mathbf{P}(\mathbf{k}) + \psi(\mathbf{x};\mathbf{k})). \quad (3.2)$$

Thus, the corrector $\psi(\mathbf{x};\mathbf{k})$ is the solution to the problem:

$$\begin{aligned}(I - (\mathcal{H}_V - E_D)^{-1}\mathcal{Q}_\perp(2i\mathbf{k} \cdot \nabla + \|\mathbf{k}\|^2 + \mu))\psi(\mathbf{x};\mathbf{k}) \\ = (\mathcal{H}_V - E_D)^{-1}\mathcal{Q}_\perp 2i\mathbf{k} \cdot \nabla \Phi(\mathbf{x})^T \mathbf{P}(\mathbf{k}),\end{aligned}$$

where \mathcal{Q}_\perp is the projection map to the orthogonal complement space of $\text{Ker}(\mathcal{H}_V - E_D)$ and

$$(\mathcal{H}_V - E_D)^{-1} : \mathcal{Q}_\perp \chi \rightarrow \mathcal{Q}_\perp H^1(\mathbb{R}^2/\mathbf{U}). \quad (3.3)$$

Here $H^1(\mathbb{R}^2/\mathbf{U})$ is the limitation of χ in $H^1(\mathbb{R}^2)$. Therefore,

$$\psi(\mathbf{x};\mathbf{k}) = ((\mathcal{H}_V - E_D)^{-1}\mathcal{Q}_\perp 2i\mathbf{k} \cdot \nabla \Phi(\mathbf{x})^T + O(\|\mathbf{k}\|^2))\mathbf{P}(\mathbf{k}).$$

Besides, from (3.2), we know that:

$$\langle \phi_l(\mathbf{x}), (\mu + 2i\mathbf{k} \cdot \nabla - \|\mathbf{k}\|^2)(\Phi(\mathbf{x})^T \mathbf{P}(\mathbf{k}) + \psi(\mathbf{x}; \mathbf{k})) \rangle = 0.$$

Based on all these, solving the original eigenvalue problem can be reduced to solving possible $\mathbf{P}(\mathbf{k})$ in $(\mu I + B(\mathbf{k}))\mathbf{P}(\mathbf{k}) = \mathbf{0}$, with

$$B(\mathbf{k}) = B_1(\mathbf{k}) + B_2(\mathbf{k}) + O(\|\mathbf{k}\|^3).$$

Here

$$B_1(\mathbf{k}) = \left(\left\langle \phi_l(\mathbf{x}), 2i\mathbf{k} \cdot \nabla \phi_j(\mathbf{x}) \right\rangle_{L^2(\Omega)} \right)_{l,j};$$

$$B_2(\mathbf{k}) = \left(\left\langle \phi_l(\mathbf{x}), (2i\mathbf{k} \cdot \nabla (\mathcal{H}_V - E_D)^{-1} \mathcal{Q}_\perp 2i\mathbf{k} \cdot \nabla - \|\mathbf{k}\|^2) \phi_j(\mathbf{x}) \right\rangle_{L^2(\Omega)} \right)_{l,j}.$$

$B(\mathbf{k})$ represents the bifurcation matrix.

1. First-order bifurcation matrix $B_1(\mathbf{k})$.

Taking advantage of the symmetry relations between $\phi_j(\mathbf{x})$ in (2.8), we can obtain [8]

$$B_1(\mathbf{k}) = \begin{pmatrix} 0 & 2i\mathbf{k} \cdot \mathbf{v}_\# & 0 & 0 \\ \overline{2i\mathbf{k} \cdot \mathbf{v}_\#} & 0 & 0 & 0 \\ 0 & 0 & 0 & -2i\mathbf{k} \cdot \mathbf{v}_\# \\ 0 & 0 & \overline{-2i\mathbf{k} \cdot \mathbf{v}_\#} & 0 \end{pmatrix}.$$

Here $\mathbf{v}_\#$ is such a quantity:

$$\mathbf{v}_\# = \langle \phi_1(\mathbf{x}), \nabla \overline{\phi_1(-\mathbf{x})} \rangle_{L^2(\Omega)} = \frac{v_F}{2} \begin{pmatrix} 1 \\ i \end{pmatrix} e^{i\theta_\#}. \quad (3.4)$$

Remark 3.1 *The eigenvalues of $b(\mathbf{k})$ are $\lambda_\pm = \pm|2i\mathbf{k} \cdot \mathbf{v}_\#| = \pm v_F \|\mathbf{k}\|$. Both λ_\pm are of multiplicity two, which means that the upper two bands near the fourfold degenerate Dirac point are tangent to each other and so do the lower two bands. To distinguish the tangent bands, we have to calculate higher-order approximations. The Fermi velocity v_F is the slope of the double Dirac cone. It is invariant under phase transformation of $\phi_1(\mathbf{x})$. The corresponding eigenvectors are determined by $\theta_\#$, which naturally changes with the phase transformation of $\phi_1(\mathbf{x})$.*

2. Second-order bifurcation matrix $B_2(\mathbf{k})$.

The second-order bifurcation matrix is Hermitian. Thus, it is enough to discuss the upper part of

$$\left(\left\langle \phi_l(\mathbf{x}), (2i\mathbf{k} \cdot \nabla (\mathcal{H}_V - E_D)^{-1} \mathcal{Q}_\perp 2i\mathbf{k} \cdot \nabla) \phi_j(\mathbf{x}) \right\rangle_{L^2(\Omega)} \right)_{l,j}.$$

First, due to

$$\begin{aligned} & \langle \phi_l(\mathbf{x}), 2i\mathbf{k} \cdot \nabla(\mathcal{H}_V - E_D)^{-1} \mathcal{Q}_\perp 2i\mathbf{k} \cdot \nabla \phi_j(\mathbf{x}) \rangle_{L^2(\Omega)} \\ &= \langle \mathcal{Q}_\perp 2i\mathbf{k} \cdot \nabla \phi_l(\mathbf{x}), (\mathcal{H}_V - E_D)^{-1} \mathcal{Q}_\perp 2i\mathbf{k} \cdot \nabla \phi_j(\mathbf{x}) \rangle_{L^2(\Omega)}, \end{aligned}$$

and the fact that $(\mathcal{H}_V - E_D)^{-1}$ is an elliptic and Hermitian operator on the periodic function space $\mathcal{Q}_\perp L^2(\Omega)$, $\langle \phi_l(\mathbf{x}), \dots \phi_l(\mathbf{x}) \rangle_{L^2(\Omega)}$ are real for all l . Besides, using the symmetries between the eigenfunctions in Theorem 2.4, $\langle \phi_l(\mathbf{x}), \dots \phi_l(\mathbf{x}) \rangle_{L^2(\Omega)}$ are the same for all l . This means the diagonal elements of the two-order bifurcation matrix are just real multiples of the identity. For other elements, because the translation operator \mathcal{V}_1 is a unitary operator and commutative with both ∇ and $(\mathcal{H}_V - E_D)^{-1}$ on $L^2(\Omega)$, we have

$$\langle \phi_l(\mathbf{x}), \dots \phi_j(\mathbf{x}) \rangle_{L^2(\Omega)} = \langle \mathcal{V}_1 \phi_l(\mathbf{x}), \dots \mathcal{V}_1 \phi_j(\mathbf{x}) \rangle_{L^2(\Omega)}.$$

Because all $\phi_l(\mathbf{x})$ are eigenfunctions of \mathcal{V}_1 , it turns out that the two-order bifurcation matrix is quasi-diagonal:

$$\begin{aligned} 0 &= \langle \phi_1(\mathbf{x}), \dots \phi_3(\mathbf{x}) \rangle_{L^2(\Omega)} = \langle \phi_1(\mathbf{x}), \dots \phi_4(\mathbf{x}) \rangle_{L^2(\Omega)} \\ &= \langle \phi_2(\mathbf{x}), \dots \phi_3(\mathbf{x}) \rangle_{L^2(\Omega)} = \langle \phi_2(\mathbf{x}), \dots \phi_4(\mathbf{x}) \rangle_{L^2(\Omega)}. \end{aligned}$$

Therefore, the second order bifurcation matrix $B_2(\mathbf{k})$ is equal to:

$$\begin{pmatrix} m(\mathbf{k}) - \|\mathbf{k}\|^2 & b(\mathbf{k}) & 0 & 0 \\ \overline{b(\mathbf{k})} & m(\mathbf{k}) - \|\mathbf{k}\|^2 & 0 & 0 \\ 0 & 0 & m(\mathbf{k}) - \|\mathbf{k}\|^2 & b(\mathbf{k}) \\ 0 & 0 & \overline{b(\mathbf{k})} & m(\mathbf{k}) - \|\mathbf{k}\|^2 \end{pmatrix}.$$

where

$$m(\mathbf{k}) = \langle \phi_1(\mathbf{x}), 2i\mathbf{k} \cdot \nabla(\mathcal{H}_V - E_D)^{-1} \mathcal{Q}_\perp 2i\mathbf{k} \cdot \nabla \phi_1(\mathbf{x}) \rangle_{L^2(\Omega)}; \quad (3.5)$$

$$b(\mathbf{k}) = \langle \phi_1(\mathbf{x}), 2i\mathbf{k} \cdot \nabla(\mathcal{H}_V - E_D)^{-1} \mathcal{Q}_\perp 2i\mathbf{k} \cdot \nabla \overline{\phi_1(-\mathbf{x})} \rangle_{L^2(\Omega)}. \quad (3.6)$$

Remark 3.2 $m(\mathbf{k})$ is real. The diagonal part $(m(\mathbf{k}) - \|\mathbf{k}\|^2)I$ of this matrix does no contribution to bifurcation. The term resulting in second-order bifurcation of the upper or lower two bands is $b(\mathbf{k})$.

Remark 3.3 Both the first-order and second-order bifurcation matrices are quasi-diagonal.

This is because the eigenvalue problems of super honeycomb lattice potential on $\bigcup_{* \in \{1, \tau, \bar{\tau}\}} \chi_{\tau, *}$

and $\bigcup_{* \in \{1, \tau, \bar{\tau}\}} \chi_{\bar{\tau}, *}$ are decoupled.

Taking use of these discussions, we finally obtain second-order accurate near-energy approximations of the four branches intersecting at the Γ point as the following theorem:

Theorem 3.4 (Double Dirac cone at the Γ point) *Let $\mathcal{H}_V = -\Delta + V(\mathbf{x})$ be a Schrödinger operator with a super honeycomb lattice potential $V(\mathbf{x})$. Assume that it has a fourfold degeneracy at the Γ point as in (2.7) and the corresponding four eigenstates $\{\phi_l(\mathbf{x})\}$ satisfy the symmetry condition (2.8). Let \mathbf{v}_\sharp , $m(\mathbf{k})$, and $b(\mathbf{k})$ denote the same terms as in (3.4), (3.5) and (3.6). Suppose that \mathbf{v}_\sharp satisfies the non-degeneracy condition:*

$$v_F = \|\mathbf{v}_\sharp\| = \|\langle \phi_1(\mathbf{x}), \nabla \overline{\phi_1(-\mathbf{x})} \rangle_{L^2(\Omega)}\| \neq 0. \quad (3.7)$$

Then, the intersecting four branches behave conically near the Γ point:

$$\begin{aligned} E_{n_*+1}(\mathbf{k}) &= E_D - \check{\mu}_1(\mathbf{k}) + \|\mathbf{k}\|^2 - m(\mathbf{k}) + O(\|\mathbf{k}\|^3), \\ E_{n_*+2}(\mathbf{k}) &= E_D - \check{\mu}_2(\mathbf{k}) + \|\mathbf{k}\|^2 - m(\mathbf{k}) + O(\|\mathbf{k}\|^3), \\ E_{n_*+3}(\mathbf{k}) &= E_D + \check{\mu}_2(\mathbf{k}) + \|\mathbf{k}\|^2 - m(\mathbf{k}) + O(\|\mathbf{k}\|^3), \\ E_{n_*+4}(\mathbf{k}) &= E_D + \check{\mu}_1(\mathbf{k}) + \|\mathbf{k}\|^2 - m(\mathbf{k}) + O(\|\mathbf{k}\|^3). \end{aligned} \quad (3.8)$$

The term corresponding to the first two order bifurcation is:

$$\begin{aligned} \check{\mu}_1(\mathbf{k}) &= \max(|2i\mathbf{k} \cdot \mathbf{v}_\sharp + b(\mathbf{k})|, |2i\mathbf{k} \cdot \mathbf{v}_\sharp - b(\mathbf{k})|), \\ \check{\mu}_2(\mathbf{k}) &= \min(|2i\mathbf{k} \cdot \mathbf{v}_\sharp + b(\mathbf{k})|, |2i\mathbf{k} \cdot \mathbf{v}_\sharp - b(\mathbf{k})|). \end{aligned}$$

Remark 3.5 *The condition (3.7) guarantees that the intersecting four branches $\{\mathcal{S}_{n_*+j}(\mathbf{k})\}_{j=1,2,3,4}$ do not behave too flat near the Γ point.*

This theorem characterizes the double Dirac cone up to second-order accuracy near the fourfold degenerate point.

Suppose that $|2i\mathbf{k} \cdot \mathbf{v}_\sharp + b(\mathbf{k})| > |2i\mathbf{k} \cdot \mathbf{v}_\sharp - b(\mathbf{k})|$. The related approximations of four branches of $\mathbf{P}(\mathbf{k})$ are:

$$\begin{aligned} \mathbf{P}^{n_*+1}(\mathbf{k}) &= \begin{pmatrix} |2i\mathbf{k} \cdot \mathbf{v}_\sharp + b(\mathbf{k})| \\ \overline{2i\mathbf{k} \cdot \mathbf{v}_\sharp + b(\mathbf{k})} \\ 0 \\ 0 \end{pmatrix} + O(\|\mathbf{k}\|^3); \\ \mathbf{P}^{n_*+2}(\mathbf{k}) &= \begin{pmatrix} 0 \\ 0 \\ -|2i\mathbf{k} \cdot \mathbf{v}_\sharp - b(\mathbf{k})| \\ \overline{2i\mathbf{k} \cdot \mathbf{v}_\sharp - b(\mathbf{k})} \end{pmatrix} + O(\|\mathbf{k}\|^3); \\ \mathbf{P}^{n_*+3}(\mathbf{k}) &= \begin{pmatrix} 0 \\ 0 \\ |2i\mathbf{k} \cdot \mathbf{v}_\sharp - b(\mathbf{k})| \\ \overline{2i\mathbf{k} \cdot \mathbf{v}_\sharp - b(\mathbf{k})} \end{pmatrix} + O(\|\mathbf{k}\|^3); \\ \mathbf{P}^{n_*+4}(\mathbf{k}) &= \begin{pmatrix} -|2i\mathbf{k} \cdot \mathbf{v}_\sharp + b(\mathbf{k})| \\ \overline{2i\mathbf{k} \cdot \mathbf{v}_\sharp + b(\mathbf{k})} \\ 0 \\ 0 \end{pmatrix} + O(\|\mathbf{k}\|^3). \end{aligned}$$

Similar results can be obtained for $|2i\mathbf{k}\cdot\mathbf{v}_\sharp+b(\mathbf{k})| < |2i\mathbf{k}\cdot\mathbf{v}_\sharp-b(\mathbf{k})|$ with these $P^j(\mathbf{k})$ reordered.

3.2 Near-energy approximation along certain direction

This subsection gives the near-energy approximation along the \mathbf{l}_2 direction, which can be written in an analytic form.

For the given direction \mathbf{l}_2 , we can choose a typical $e^{i\theta^*}\phi_1(\mathbf{x})$, which is also in $\chi_{\tau,\tau}$, to replace the original $\phi_1(\mathbf{x})$, such that the new \mathbf{v}_\sharp has the following property [11]:

$$-2i\mathbf{r}\cdot\mathbf{v}_\sharp = \frac{v_F}{\|\mathbf{l}_2\|}(\mathbf{r}\cdot\mathbf{l}_2 - \text{Det}[\mathbf{r}, \mathbf{l}_2]i), \quad \mathbf{r} \in \mathbb{R}^2. \quad (3.9)$$

In the following content throughout this paper, we fix the $\phi_1(\mathbf{x})$ such that \mathbf{v}_\sharp always take such a simple form (3.9).

Proposition 3.6 (Near-energy approximation along \mathbf{l}_2 direction) *Let $V(\mathbf{x})$ be a super honeycomb lattice potential and $\mathcal{H}_V = -\Delta + V(\mathbf{x})$ be a Schrödinger operator as in Theorem 3.4. Assume (3.9) is true for \mathbf{v}_\sharp and $b(\mathbf{l}_2) \neq 0$ where $b(\mathbf{k})$ is as in (3.6). Then there exists a $\lambda_0 > 0$ such that for all $|\lambda| < \lambda_0$ the following is true:*

1. $\{E_{n_*+j}(\lambda\mathbf{l}_2)\}_{j=1,2,3,4}$ are equivalent to such four real analytic functions intersecting at $\lambda = 0$:

$$\begin{aligned} \theta_1(\lambda) &= E_D - v_F\|\mathbf{l}_2\|\lambda + r_1(\lambda)\lambda^2, \\ \theta_2(\lambda) &= E_D - v_F\|\mathbf{l}_2\|\lambda + r_2(\lambda)\lambda^2, \\ \theta_3(\lambda) &= E_D + v_F\|\mathbf{l}_2\|\lambda + r_3(\lambda)\lambda^2, \\ \theta_4(\lambda) &= E_D + v_F\|\mathbf{l}_2\|\lambda + r_4(\lambda)\lambda^2, \end{aligned} \quad (3.10)$$

with $|r_j(\lambda)| < C$, where C is a positive constant independent of λ .

2. Corresponding orthonormal eigen modes in $\text{Ker}(\mathcal{H}_V - \theta_j(\lambda))$ in $L^2_{\lambda\mathbf{l}_2}(\mathbb{R}^2/\mathbf{U})$ can be chosen real analytically dependent on λ :

$$\begin{aligned} \Theta_1(\mathbf{x}; \lambda) &= \frac{1}{\sqrt{2}}e^{i\lambda\mathbf{l}_2\cdot\mathbf{x}}(\phi_1(\mathbf{x}) - \phi_2(\mathbf{x})) + R_1(\mathbf{x}; \lambda), \\ \Theta_2(\mathbf{x}; \lambda) &= \frac{1}{\sqrt{2}}e^{i\lambda\mathbf{l}_2\cdot\mathbf{x}}(\phi_3(\mathbf{x}) + \phi_4(\mathbf{x})) + R_2(\mathbf{x}; \lambda), \\ \Theta_3(\mathbf{x}; \lambda) &= \frac{1}{\sqrt{2}}e^{i\lambda\mathbf{l}_2\cdot\mathbf{x}}(\phi_3(\mathbf{x}) - \phi_4(\mathbf{x})) + R_4(\mathbf{x}; \lambda), \\ \Theta_4(\mathbf{x}; \lambda) &= \frac{1}{\sqrt{2}}e^{i\lambda\mathbf{l}_2\cdot\mathbf{x}}(\phi_1(\mathbf{x}) + \phi_2(\mathbf{x})) + R_3(\mathbf{x}; \lambda). \end{aligned} \quad (3.11)$$

Here $R_j(\mathbf{x}; \lambda) = O_{H^2(\mathbb{R}^2/\mathbf{U})}(\lambda)$.

Remark 3.7 *The condition $b(\mathbf{l}_2) \neq 0$ makes sure that the upper two or the lower two of these four branches split at order $O(\|\mathbf{k}\|^2)$ exactly.*

Proof With (3.9), the expressions of $\theta_j(\lambda)$ and $\Theta(\mathbf{x}; \lambda)$ can be obtained directly from the discussion in the last subsection. We first solve out four $\theta_j(\lambda)$ real analytic dependent on λ

from $\det(\theta I + B(\lambda_2)) = 0$ where $B(\mathbf{k})$ is the bifurcation matrix in the last subsection, and then find the four corresponding $\Theta_j(\mathbf{x}; \lambda)$ which are also real analytically dependent on λ [13]. \square

4 Multiscale expansions of edge states

In this paper, the proof of the existence of two gapped edge states of the domain wall modulated operator $\mathcal{H}_{edge}^\delta$ can be divided into two main parts: calculating the main terms of energies and eigenstates by multiscale expansions first and estimating the remaining terms following the classical method as in the paper of Fefferman and Weinstein [13] then. This section focuses on calculating the main terms. The most important conclusion in this section is the existence of the gap of order $O(\delta^2)$ under natural assumptions on second-order bifurcation terms. Specifically, we can expand the energies of these two edge states at $k_{\parallel} = 0$ as

$$\mathcal{E}_j(0) = E_D + \delta \mathcal{E}_j^{(1)}(0) + \delta^2 \mathcal{E}_j^{(2)}(0) + O(\delta^3).$$

The two main conclusions in this part are:

- the linear terms $\mathcal{E}_j^{(1)}(0)$ are both zero for $j = 1, 2$, and they correspond to a two-dimensional zero energy eigenspace of an operator which can be diagonalized into two Dirac operators;
- the quadratic terms $\mathcal{E}_j^{(2)}(0)$ bifurcate when second-order bifurcation term (4.24) is nonzero, which coincides with the non-degeneracy condition of order $O(\|\mathbf{k}\|^2)$ bifurcation matrix; see the last section.

Let us take a more convenient direction $\tilde{\mathbf{l}}_1 = \mathbf{l}_1 - \frac{\mathbf{l}_1 \cdot \mathbf{l}_2}{\|\mathbf{l}_2\|^2} \mathbf{l}_2$, which is orthogonal to \mathbf{l}_2 and satisfies $\tilde{\mathbf{l}}_1 \cdot \mathbf{w}_1 = 2\pi$. Let $k_{\parallel} = \delta s \tilde{\mathbf{l}}_1 \cdot \mathbf{w}_1$, and denote:

$$\check{L}_s^2(\mathbb{R}^2 / \mathbb{Z}\mathbf{w}_1) = \{f \in L^2(\Omega_e) \mid f(\mathbf{x}) = e^{i\delta s \tilde{\mathbf{l}}_1 \cdot \mathbf{x}} p(\mathbf{x}), \quad p(\mathbf{x} + \mathbf{w}_1) = p(\mathbf{x})\}.$$

In this section, we aim to solve the following eigenvalue problem by multiscale expansions:

$$\mathcal{H}_{edge}^\delta \psi(\mathbf{x}; s) = \mathcal{E}(s) \psi(\mathbf{x}, s), \quad \psi(\mathbf{x}; s) \in \check{L}_s^2(\mathbb{R}^2 / \mathbb{Z}\mathbf{w}_1). \quad (4.1)$$

For simplicity, we denote the space of \mathbf{w}_1 -periodic functions:

$$\chi_e = \check{L}_0^2(\mathbb{R}^2 / \mathbb{Z}\mathbf{w}_1) = \{f \in L^2(\Omega_e) \mid f(\mathbf{x} + \mathbf{w}_1) = f(\mathbf{x})\}. \quad (4.2)$$

For δ small, s near zero, and $\mathcal{E}(s)$ near E_D , using the slow variable $\zeta = \delta \mathbf{l}_2 \cdot \mathbf{x}$ and associated multiscale solution $\psi(\mathbf{x}, \zeta; s)$. Expand the solution in powers of δ :

$$\begin{aligned} \psi(\mathbf{x}, \zeta; s) &= \psi^{(0)}(\mathbf{x}, \zeta; s) + \delta \psi^{(1)}(\mathbf{x}, \zeta; s) + \delta^2 \psi^{(2)}(\mathbf{x}, \zeta; s) + \dots, \\ \mathcal{E}(s) &= E_D + \delta \mathcal{E}^{(1)}(s) + \delta^2 \mathcal{E}^{(2)}(s) + \dots \end{aligned} \quad (4.3)$$

Then, substituting the powers into the equation and grouping the terms by order in δ to obtain equations for these $\psi^{(j)}(\mathbf{x}, \zeta, s)$ and $\mathcal{E}^{(j)}$.

At order $O(1)$, it is:

$$(\mathcal{H}_V - E_D)\psi^{(0)}(\mathbf{x}, \zeta; s) = 0, \quad (4.4)$$

where $\mathcal{H}_V = -\Delta_{\mathbf{x}} + V(\mathbf{x})$.

At order $O(\delta)$, it is:

$$(\mathcal{H}_V - E_D)\psi^{(1)}(\mathbf{x}, \zeta; s) = \mathcal{L}_1(s)\psi^{(0)}(\mathbf{x}, \zeta; s), \quad (4.5)$$

where $\mathcal{L}_1(s) = 2(is\tilde{\mathbf{l}}_1 + \partial_\zeta \mathbf{l}_2) \cdot \nabla_{\mathbf{x}} - \eta(\zeta)W(\mathbf{x}) + \mathcal{E}^{(1)}(s)$.

At order $O(\delta^2)$, it is:

$$(\mathcal{H}_V - E_D)\psi^{(2)}(\mathbf{x}, \zeta; s) = \mathcal{L}_1(s)\psi^{(1)}(\mathbf{x}, \zeta; s) + \mathcal{L}_2(s)\psi^{(0)}(\mathbf{x}, \zeta; s), \quad (4.6)$$

where $\mathcal{L}_2(s) = (is\tilde{\mathbf{l}}_1 + \partial_\zeta \mathbf{l}_2)^2 + \mathcal{E}^{(2)}(s)$.

At order $O(\delta^n)$, $n \geq 3$, it is:

$$\begin{aligned} & (\mathcal{H}_V - E_D)\psi^{(n)}(\mathbf{x}, \zeta; s) \\ &= \mathcal{L}_1(s)\psi^{(n-1)}(\mathbf{x}, \zeta; s) + \mathcal{L}_2(s)\psi^{(n-2)}(\mathbf{x}, \zeta; s) + \sum_{j=3}^n \mathcal{E}^{(j)}(s)\psi^{(n-j)}(\mathbf{x}, \zeta; s). \end{aligned} \quad (4.7)$$

4.1 Order $O(\delta)$ terms

For equation (4.4), we can use the ansatz

$$\psi^{(0)}(\mathbf{x}, \zeta; s) = \Phi(\mathbf{x})^T \boldsymbol{\alpha}(\zeta; s), \quad (4.8)$$

where $\boldsymbol{\alpha}(\zeta; s) = (\alpha_1(\zeta; s), \alpha_2(\zeta; s), \alpha_3(\zeta; s), \alpha_4(\zeta; s))^T$, and $\Phi(\mathbf{x})$ as in (3.1). Substituting the ansatz into (4.5), by the solvable condition for $(\mathcal{H}_V - E_D)$, the right-hand side of (4.5) should be orthogonal to $\text{Ker}(\mathcal{H}_V - E_D)$:

$$\langle \Phi(\mathbf{x}), \mathcal{L}_1(s)\Phi(\mathbf{x})^T \rangle_{L^2(\Omega)} \boldsymbol{\alpha}(\zeta; s) = 0; \quad (4.9)$$

to be specific:

$$\begin{aligned} 0 = & 2\langle \Phi(\mathbf{x}), \nabla_{\mathbf{x}}\Phi(\mathbf{x})^T \rangle_{L^2(\Omega)} \cdot \left(is\tilde{\mathbf{l}}_1 \boldsymbol{\alpha}(\zeta; s) + \partial_\zeta \boldsymbol{\alpha}(\zeta; s) \mathbf{l}_2 \right) \\ & + \mathcal{E}^{(1)} \langle \Phi(\mathbf{x}), \Phi(\mathbf{x})^T \rangle_{L^2(\Omega)} \boldsymbol{\alpha}(\zeta; s) - \langle \Phi(\mathbf{x}), W(\mathbf{x})\Phi(\mathbf{x})^T \rangle_{L^2(\Omega)} \eta(\zeta) \boldsymbol{\alpha}(\zeta; s). \end{aligned} \quad (4.10)$$

With the help of (3.9), (2.9), and (2.8) the symmetric relations between $\phi_j(\mathbf{x})$, (4.10) is such an equation:

$$(\mathcal{D}(s) - \mathcal{E}^{(1)}(s)I)\boldsymbol{\alpha}(\zeta; s) = 0, \quad (4.11)$$

where

$$\mathcal{D}(s) = \text{Det}[\tilde{\mathbf{l}}_1, \mathbf{l}_2] \frac{v_F}{\|\mathbf{l}_2\|} s\sigma_3 \otimes \sigma_2 + \frac{1}{i} v_F \|\mathbf{l}_2\| \sigma_3 \otimes \sigma_1 \partial_\zeta + c_{\#} \eta(\zeta) \sigma_1 \otimes I. \quad (4.12)$$

σ_j are pauli matrices.

Use the following orthogonal transformation Q to decouple the original 4-dimensional problem (4.11) into two 2-dimensional problems:

$$Q = \begin{pmatrix} \frac{\sqrt{2}}{2} & & \frac{\sqrt{2}}{2} & \\ & \frac{\sqrt{2}}{2} & & \frac{\sqrt{2}}{2} \\ \frac{\sqrt{2}}{2} & & -\frac{\sqrt{2}}{2} & \\ & -\frac{\sqrt{2}}{2} & & \frac{\sqrt{2}}{2} \end{pmatrix}. \quad (4.13)$$

Then the effective Dirac operator for order $O(\delta)$ is

$$\tilde{\mathcal{D}}(s) = Q^T \mathcal{D}(s) Q = \text{diag}(\mathcal{D}_1(s), \mathcal{D}_2(s)), \quad (4.14)$$

where

$$\begin{aligned} \mathcal{D}_1(s) &= \text{Det}[\tilde{\mathbf{l}}_1, \mathbf{l}_2] \frac{v_F}{\|\mathbf{l}_2\|} s \sigma_2 + \frac{1}{i} v_F \|\mathbf{l}_2\| \sigma_1 \partial_\zeta + c_\# \eta(\zeta) \sigma_3, \\ \mathcal{D}_2(s) &= \text{Det}[\tilde{\mathbf{l}}_1, \mathbf{l}_2] \frac{v_F}{\|\mathbf{l}_2\|} s \sigma_2 + \frac{1}{i} v_F \|\mathbf{l}_2\| \sigma_1 \partial_\zeta - c_\# \eta(\zeta) \sigma_3. \end{aligned} \quad (4.15)$$

Thus, solving eigenvalue problem (4.11) is equivalent to finding eigenvalues of $\mathcal{D}_1(s)$ and $\mathcal{D}_2(s)$. Note that $\mathcal{D}_2(s) = -\overline{\mathcal{D}_1(s)}$. We have the following proposition for the eigenvalue and eigenfunctions for $\mathcal{D}_1(s)$ and $\mathcal{D}_2(s)$. Its proof is simple, and we omit it here.

Proposition 4.1 (First-order approximation of the edge states) $\mathcal{D}_1(s)$ has a simple eigenvalue

$$\mu(s) = \text{sgn}(c_\#) \text{Det}[\tilde{\mathbf{l}}_1, \mathbf{l}_2] \frac{v_F}{\|\mathbf{l}_1\|} s$$

with the normalized eigenstate:

$$\mathbf{d}(\zeta) = \begin{pmatrix} \text{sgn}(c_\#) \\ i \end{pmatrix} \alpha_\#(\zeta),$$

where

$$\alpha_\#(\zeta) = c_\alpha \exp\left(-\frac{|c_\#|}{v_F \|\mathbf{l}_2\|} \int_0^\zeta \eta(t) dt\right), \quad (4.16)$$

and c_α is a real normalization coefficient for $\mathbf{d}(\zeta)$. Similarly, $\mathcal{D}_2(s)$ has a simple eigenvalue $-\mu(s)$ with the eigenstate $\overline{\mathbf{d}(\zeta)}$.

We can deduce the following conclusions from this proposition.

1. When $s \neq 0$, $\mathcal{D}(s)$ has two different eigenvalues $\mathcal{E}_1^{(1)}(s) = \mu(s)$ and $\mathcal{E}_2^{(1)}(s) = -\mu(s)$, and corresponding eigenstates:

$$\boldsymbol{\alpha}^1(\zeta; s) = Q^T \begin{pmatrix} \mathbf{d}(\zeta) \\ 0 \\ 0 \end{pmatrix}; \quad \boldsymbol{\alpha}^2(\zeta; s) = Q^T \begin{pmatrix} 0 \\ 0 \\ \overline{\mathbf{d}(\zeta)} \end{pmatrix}.$$

2. **(The first-order degeneracy of the edge states' energies)** When $s = 0$, 0 is an eigenvalue of $\mathcal{D}(0)$ of multiplicity two with such a pair of eigenstates as a basis:

$$\boldsymbol{\alpha}^1(\zeta; 0) = \alpha_{\sharp}(\zeta) \begin{pmatrix} \text{sgn}(c_{\sharp}) \\ 0 \\ 0 \\ -i \end{pmatrix}, \quad \boldsymbol{\alpha}^2(\zeta; 0) = \alpha_{\sharp}(\zeta) \begin{pmatrix} 0 \\ \text{sgn}(c_{\sharp}) \\ -i \\ 0 \end{pmatrix}, \quad (4.17)$$

Note that we choose two special orthogonal $\boldsymbol{\alpha}^l(\zeta; 0)$ in $\text{Ker}(\mathcal{D}(0))$ here to simplify the calculation in the next subsection.

Thus, for $s \neq 0$, we have two different solutions at order $O(\delta)$ as above and we can take $\psi_j^{(0)}(\mathbf{x}, \zeta; s) = \Phi(\mathbf{x})^T \boldsymbol{\alpha}^j(\zeta; s)$ for $j = 1, 2$ respectively.

But for $s = 0$, $\mathcal{E}^{(1)}(0) = 0$ is of multiplicity two, and we can only distinguish the two eigenvalues and corresponding eigenstates at higher orders. Now we just set

$$\psi^{(0)}(\mathbf{x}, \zeta; 0) = c^1 \Phi(\mathbf{x})^T \boldsymbol{\alpha}^1(\zeta; 0) + c^2 \Phi(\mathbf{x})^T \boldsymbol{\alpha}^2(\zeta; 0) \quad (4.18)$$

and try to solve out two groups of (c^1, c^2) at the next order.

4.2 Order $O(\delta^2)$ terms

If $\psi^{(0)}(\mathbf{x}, \zeta; s)$ is solved out, we can recursively use the ansatz

$$\psi^{(1)}(\mathbf{x}, \zeta; s) = \Phi(\mathbf{x})^T \boldsymbol{\beta}(\zeta, s) + (\mathcal{H}_V - E_D)^{-1} \mathcal{L}_1(s) \psi^{(0)}(\mathbf{x}, \zeta; s). \quad (4.19)$$

where $\boldsymbol{\beta}(\zeta; s) = (\beta_1(\zeta; s), \beta_2(\zeta; s), \beta_3(\zeta; s), \beta_4(\zeta; s))^T$, and $(\mathcal{H}_V - E_D)^{-1}$ is as in (3.3).

For $s \neq 0$, the original multiscale eigenvalue problem is split into two different problems whose eigenvalue has the first-order term of $\mu(s)\delta$ and $-\mu(s)\delta$ respectively, and the rest work is just in a traditional style. At order $O(\delta^2)$, using the ansatz (4.19), we can obtain

$$(\mathcal{H}_V - E_D) \psi^{(2)}(\mathbf{x}, \zeta; s) = \mathcal{L}_1(s) \Phi(\mathbf{x})^T \boldsymbol{\beta}(\zeta; s) + \mathcal{F}(s) \psi_j^{(0)}(\mathbf{x}, \zeta; s),$$

where $\mathcal{F}(s) = \mathcal{L}_1(s)(\mathcal{H}_V - E_D)^{-1} \mathcal{L}_1(s) + \mathcal{L}_2(s)$. Use the solvable condition of $(\mathcal{H}_V - E_D)$ again to solve out $\boldsymbol{\beta}_j(\zeta; s)$ and construct ansatzes like (4.19) recursively for all the rest orders to get the multiscale expansions of two gapped eigenvalues $\mathcal{E}_1(s)$ and $\mathcal{E}_2(s)$ and associated eigenstates $\psi_1(\mathbf{x}, \zeta; s)$ and $\psi_2(\mathbf{x}, \zeta; s)$.

However, for $s = 0$, at order $O(\delta^2)$, we can only obtain:

$$\begin{aligned} (\mathcal{H}_V - E_D) \psi^{(2)}(\mathbf{x}, \zeta; 0) &= \mathcal{L}_1(0) \Phi(\mathbf{x})^T \boldsymbol{\beta}_j(\zeta; 0) \\ &+ \mathcal{F}(0) (c^1 \Phi(\mathbf{x})^T \boldsymbol{\alpha}^1(\zeta; 0) + c^2 \Phi(\mathbf{x})^T \boldsymbol{\alpha}^2(\zeta; 0)). \end{aligned} \quad (4.20)$$

Similarly, (4.20) has to satisfy the solvable condition of $(\mathcal{H}_V - E_D)$. Thus, the right-hand side of the equation is orthogonal to $\text{Ker}(\mathcal{H}_V - E_D)$, and we can obtain:

$$\mathcal{D}(0) \boldsymbol{\beta}(\zeta; 0) = -\langle \Phi(\mathbf{x}), \mathcal{F}(0) (c^1 \Phi(\mathbf{x})^T \boldsymbol{\alpha}^1(\zeta; 0) + c^2 \Phi(\mathbf{x})^T \boldsymbol{\alpha}^2(\zeta; 0)) \rangle_{L^2(\Omega)}. \quad (4.21)$$

Because $\mathcal{D}(0)$ is self-adjoint, (4.21) has a solution if and only if the right-hand side is orthogonal to $\boldsymbol{\alpha}^l(\zeta; 0)$ for $l = 1, 2$:

$$\begin{aligned} & \langle \boldsymbol{\alpha}^l(\zeta; 0), \langle \Phi(\mathbf{x}), \mathcal{F}(0)\Phi(\mathbf{x})^T \boldsymbol{\alpha}^1(\zeta; 0) \rangle_{L^2(\Omega)} \rangle_{L^2(\mathbb{R})} c^1 \\ & + \langle \boldsymbol{\alpha}^l(\zeta; 0), \langle \Phi(\mathbf{x}), \mathcal{F}(0)\Phi(\mathbf{x})^T \boldsymbol{\alpha}^2(\zeta; 0) \rangle_{L^2(\Omega)} \rangle_{L^2(\mathbb{R})} c^2 = 0. \end{aligned} \quad (4.22)$$

The outer inner product is about ζ in $L^2(\mathbb{R})$. This equation has nonzero solutions $(c^1, c^2)^T$ if and only if $\text{Det } B_e = 0$, where

$$B_e = \left\langle \begin{pmatrix} \boldsymbol{\alpha}^1(\zeta; 0) \\ \boldsymbol{\alpha}^2(\zeta; 0) \end{pmatrix}, \langle \Phi(\mathbf{x}), \mathcal{F}(0)\Phi(\mathbf{x})^T \begin{pmatrix} \boldsymbol{\alpha}^1(\zeta; 0) & \boldsymbol{\alpha}^2(\zeta; 0) \end{pmatrix} \rangle_{L^2(\Omega)} \right\rangle_{L^2(\mathbb{R})}. \quad (4.23)$$

B_e is the bifurcation matrix for the edge states' problem with the following property.

Proposition 4.2 (Second-order approximation of the edge states) *Det $B_e = 0$ has two real solutions $\mathcal{E}_1^{(2)}(0)$ and $\mathcal{E}_2^{(2)}(0)$.*

Proof From (4.23), we know that

$$B_e = \mathcal{E}^{(2)}(0)I + \left\langle \begin{pmatrix} \boldsymbol{\alpha}^1(\zeta; 0) \\ \boldsymbol{\alpha}^2(\zeta; 0) \end{pmatrix}, \langle \Phi(\mathbf{x}), \mathcal{N}\Phi(\mathbf{x})^T \begin{pmatrix} \boldsymbol{\alpha}^1(\zeta; 0) & \boldsymbol{\alpha}^2(\zeta; 0) \end{pmatrix} \rangle_{L^2(\Omega)} \right\rangle_{L^2(\mathbb{R})}.$$

Here $\mathcal{N} = (2\partial_\zeta \mathbf{l}_2 \cdot \nabla_{\mathbf{x}} - \eta(\zeta)W(\mathbf{x}))(\mathcal{H}_V - E_D)^{-1} \mathcal{Q}_\perp (2\partial_\zeta \mathbf{l}_2 \cdot \nabla_{\mathbf{x}} - \eta(\zeta)W(\mathbf{x})) + (\partial_\zeta \mathbf{l}_2)^2$. Denote $\mathcal{N}_1 = 2\mathbf{l}_2 \cdot \nabla(\mathcal{H}_V - E_D)^{-1} \mathcal{Q}_\perp 2\mathbf{l}_2 \cdot \nabla$, $\mathcal{N}_2 = 2\mathbf{l}_2 \cdot \nabla(\mathcal{H}_V - E_D)^{-1} \mathcal{Q}_\perp W(\mathbf{x})$, $\mathcal{N}_3 = W(\mathbf{x})(\mathcal{H}_V - E_D)^{-1} \mathcal{Q}_\perp 2\mathbf{l}_2 \cdot \nabla$, and $\mathcal{N}_4 = W(\mathbf{x})(\mathcal{H}_V - E_D)^{-1} \mathcal{Q}_\perp W(\mathbf{x})$. Now, let us calculate the following terms first.

1. $\left(\langle \phi_l(\mathbf{x}), \mathcal{N}_1 \phi_j(\mathbf{x}) \rangle_{L^2(\Omega)} \right)_{l,j}$:

This can be calculated similarly with second-order bifurcation terms in section 3.1. The final result is

$$\left(\langle \phi_l(\mathbf{x}), \mathcal{N}_1 \phi_j(\mathbf{x}) \rangle_{L^2(\Omega)} \right)_{l,j} = m_1 I + I \otimes M_1.$$

Here $M_1 = \begin{pmatrix} 0 & b_1 \\ \bar{b}_1 & 0 \end{pmatrix}$, where $b_1 = \langle \phi_1(\mathbf{x}), \mathcal{N}_1 \phi_2(\mathbf{x}) \rangle_{L^2(\Omega)}$.

2. $\left(\langle \phi_l(\mathbf{x}), \mathcal{N}_2 \phi_j(\mathbf{x}) \rangle_{L^2(\Omega)} \right)_{l,j}$:

Because \mathcal{R} is unitary, we have:

$$\begin{aligned} & \langle \phi_l(\mathbf{x}), \nabla(\mathcal{H}_V - E_D)^{-1} \mathcal{Q}_\perp W(\mathbf{x}) \phi_j(\mathbf{x}) \rangle_{L^2(\Omega)} \\ & = \langle \mathcal{R}(\phi_l(\mathbf{x})), \mathcal{R}(\nabla(\mathcal{H}_V - E_D)^{-1} \mathcal{Q}_\perp W(\mathbf{x}) \phi_j(\mathbf{x})) \rangle_{L^2(\Omega)} \\ & = R^* \langle \mathcal{R}(\phi_l(\mathbf{x})), \nabla(\mathcal{H}_V - E_D)^{-1} \mathcal{Q}_\perp W(\mathbf{x}) \mathcal{R}(\phi_j(\mathbf{x})) \rangle_{L^2(\Omega)}. \end{aligned}$$

Since $\phi_j(\mathbf{x})$ and $\phi_l(\mathbf{x})$ are eigenfunctions of \mathcal{R} , the above quantity takes a nonzero vector only when it is an eigenvector of R^* with eigenvalue τ or $\bar{\tau}$, which means $\phi_j(\mathbf{x})$

and $\phi_l(\mathbf{x})$ should correspond to different eigenvalues of \mathcal{R} . By the symmetries between the eigenfunctions in Theorem 2.4, we can get:

$$\left(\langle \phi_l(\mathbf{x}), \mathcal{N}_2 \phi_j(\mathbf{x}) \rangle_{L^2(\Omega)} \right)_{l,j} = \sigma_3 \otimes M_2 + \frac{1}{i} \sigma_2 \otimes M_3,$$

where

$$M_2 = \begin{pmatrix} 0 & b_2 \\ -\overline{b_2} & 0 \end{pmatrix} \quad M_3 = \begin{pmatrix} 0 & -b_3 \\ \overline{b_3} & 0 \end{pmatrix}.$$

$$b_2 = \langle \phi_1(\mathbf{x}), \mathcal{N}_2 \phi_2(\mathbf{x}) \rangle_{L^2(\Omega)} \text{ and } b_3 = \langle \phi_1(\mathbf{x}), \mathcal{N}_2 \phi_4(\mathbf{x}) \rangle_{L^2(\Omega)}.$$

$$3. \left(\langle \phi_l(\mathbf{x}), \mathcal{N}_3 \phi_j(\mathbf{x}) \rangle_{L^2(\Omega)} \right)_{l,j} :$$

Note that

$$\begin{aligned} \langle \phi_l(\mathbf{x}), \mathcal{N}_3 \phi_j(\mathbf{x}) \rangle_{L^2(\Omega)} &= \langle -\mathcal{N}_2 \phi_l(\mathbf{x}), \phi_j(\mathbf{x}) \rangle_{L^2(\Omega)} \\ &= -\overline{\langle \phi_j(\mathbf{x}), \mathcal{N}_2 \phi_l(\mathbf{x}) \rangle_{L^2(\Omega)}}. \end{aligned}$$

$$\text{Thus, } \left(\langle \phi_l(\mathbf{x}), \mathcal{N}_3 \phi_j(\mathbf{x}) \rangle_{L^2(\Omega)} \right)_{l,j} = -\left(\langle \phi_l(\mathbf{x}), \mathcal{N}_2 \phi_j(\mathbf{x}) \rangle_{L^2(\Omega)} \right)_{l,j}^H.$$

$$4. \left(\langle \phi_l(\mathbf{x}), \mathcal{N}_4 \phi_j(\mathbf{x}) \rangle_{L^2(\Omega)} \right)_{l,j} :$$

Again because \mathcal{R} is unitary, $\langle \phi_l(\mathbf{x}), \mathcal{N}_4 \phi_j(\mathbf{x}) \rangle_{L^2(\Omega)}$ takes a nonzero value only when $\phi_j(\mathbf{x})$ and $\phi_l(\mathbf{x})$ correspond to the same eigenvalue of \mathcal{R} . Denote

$$m_4 = \langle \phi_1(\mathbf{x}), \mathcal{N}_4 \phi_1(\mathbf{x}) \rangle_{L^2(\Omega)};$$

$$b_4 = \langle \phi_1(\mathbf{x}), \mathcal{N}_4 \phi_3(\mathbf{x}) \rangle_{L^2(\Omega)}.$$

Then, due to the fact that \mathcal{N}_4 is Hermitian and the symmetries between $\phi_l(\mathbf{x})$, m_4 is real and $\langle \phi_l(\mathbf{x}), \mathcal{N}_4 \phi_l(\mathbf{x}) \rangle_{L^2(\Omega)} = m_4$ for all l . \mathcal{P} is unitary, too. Thus,

$$\begin{aligned} b_4 &= \langle \phi_1(\mathbf{x}), \mathcal{N}_4 \phi_3(\mathbf{x}) \rangle_{L^2(\Omega)} = \langle \mathcal{P} \phi_1(\mathbf{x}), \mathcal{P} \mathcal{N}_4 \phi_3(\mathbf{x}) \rangle_{L^2(\Omega)} \\ &= \langle \phi_3(\mathbf{x}), \mathcal{N}_4 \phi_1(\mathbf{x}) \rangle_{L^2(\Omega)} = \langle \mathcal{N}_4 \phi_3(\mathbf{x}), \phi_1(\mathbf{x}) \rangle_{L^2(\Omega)} \end{aligned}$$

is real. The final result is:

$$\left(\langle \phi_l(\mathbf{x}), \mathcal{N}_4 \phi_j(\mathbf{x}) \rangle_{L^2(\Omega)} \right)_{l,j} = m_4 I + \sigma_1 \otimes M_4,$$

where $M_4(\mathbf{k}) = b_4 I$.

Based on these and the expressions of $\boldsymbol{\alpha}^l(\zeta)$, we can finally get that:

$$B_e = (\mathcal{E}^{(2)}(0) + m_0)I + b_0 \sigma_1.$$

Here m_0 and b_0 are such real numbers:

$$\begin{aligned} m_0 &= 2m_1 \langle \alpha_{\#}(\zeta), \partial_{\zeta}^2 \alpha_{\#}(\zeta) \rangle_{L^2(\mathbb{R})} - 4 \operatorname{sgn}(c_{\#}) \Im(b_3) \langle \alpha_{\#}(\zeta), \partial_{\zeta}(\eta(\zeta) \alpha_{\#}(\zeta)) \rangle_{L^2(\mathbb{R})} \\ &\quad + 2m_4 \langle \alpha_{\#}(\zeta), \eta(\zeta)^2 \alpha_{\#}(\zeta) \rangle_{L^2(\mathbb{R})} + 2 \langle \alpha_{\#}(\zeta), \partial_{\zeta}^2 \alpha_{\#}(\zeta) \rangle_{L^2(\mathbb{R})}; \\ b_0 &= 2\Re(b_1) \langle \alpha_{\#}(\zeta), \partial_{\zeta}^2 \alpha_{\#}(\zeta) \rangle_{L^2(\mathbb{R})}. \end{aligned}$$

Thus, $\operatorname{Det} B_e = 0$ has two real solutions $\mathcal{E}_1^{(2)}(0) = -m_0 + b_0$ and $\mathcal{E}_1^{(2)}(0) = -m_0 - b_0$. \square

(The second-order bifurcation of edge states' energies) These two solutions are different if and only if:

$$\Re \left(\langle \phi_1(\mathbf{x}), 2\mathbf{l}_2 \cdot \nabla (\mathcal{H}_V - E_D)^{-1} \mathcal{Q}_{\perp} 2\mathbf{l}_2 \cdot \nabla \overline{\phi_1(-\mathbf{x})} \rangle_{L^2(\Omega)} \right) \neq 0, \quad (4.24)$$

and

$$\langle \alpha_{\#}(\zeta), \partial_{\zeta}^2 \alpha_{\#}(\zeta) \rangle_{L^2(\mathbb{R})} \neq 0. \quad (4.25)$$

Note that $\langle \alpha_{\#}(\zeta), \partial_{\zeta}^2 \alpha_{\#}(\zeta) \rangle_{L^2(\mathbb{R})} = 0$ if and only if $\partial_{\zeta} \alpha_{\#}(\zeta) = 0$ is true for almost all $\zeta \in \mathbb{R}$, which is certainly not true. Assume the condition (4.24) is true throughout the following discussion so that the two edge states separate at order $O(\delta^2)$. Then we can solve (c_1^1, c_1^2) and (c_2^1, c_2^2) for equation (4.22), and $\beta_1(\zeta; 0)$ and $\beta_2(\zeta; 0)$ for equation (4.21) related to $\mathcal{E}_1^{(2)}(0)$ and $\mathcal{E}_2^{(2)}(0)$ respectively.

4.3 Order $O(\delta^n)$ terms

For edge states with separated energies, repeat using ansatz similar to (4.19) and the solvable conditions for order $O(\delta^n)$ can solve the multiscale problem recursively. The critical fact is that there are two independent eigenvalue problems with eigenvalues differing from at least at order $O(\delta^2)$.

5 Rigorous formulation of two gapped edge states

Based on the preparation in the last two sections, we are now ready to establish the existence of two gapped edge states at $k_{\parallel} = 0$ rigorously. Recall that χ_e is the function space at $k_{\parallel} = 0$; see (4.2). The main theorem stating the existence of two edge states in χ_e is below.

Theorem 5.1 (Existence of the gapped edge states) *Let $H_V = -\Delta + V(\mathbf{x})$ be a bulk Hamiltonian as in Theorem 3.4, $H^{\delta} = -\Delta + V(\mathbf{x}) + \delta W(\mathbf{x})$ be a bulk Hamiltonian as in Theorem 2.6, and the folding symmetry breaking domain wall modulated edge operator $\mathcal{H}_{edge}^{\delta} = -\Delta + V(\mathbf{x}) + \delta \eta(\delta \mathbf{l}_2 \cdot \mathbf{x}) W(\mathbf{x})$ be as in Definition 2.9. Suppose that when $\phi_1(\mathbf{x})$ is chosen to satisfy (3.9), the corresponding second-order non-degeneracy condition*

$$\Re \left(\langle \phi_1(\mathbf{x}), 2\mathbf{l}_2 \cdot \nabla (\mathcal{H}_V - E_D)^{-1} \mathcal{Q}_{\perp} 2\mathbf{l}_2 \cdot \nabla \overline{\phi_1(-\mathbf{x})} \rangle_{L^2(\Omega)} \right) \neq 0 \quad (5.1)$$

is true. Then there exists $\delta_0 > 0$, such that for all $0 < \delta < \delta_0$, $\mathcal{H}_{edge}^{\delta}$ has two eigen pairs $(\mathcal{E}_1, \psi_1(\mathbf{x}))$ and $(\mathcal{E}_2, \psi_2(\mathbf{x}))$ in χ_e satisfying:

1. the energies \mathcal{E}_1 and \mathcal{E}_2 are near E_D and gapped of order $O(\delta^2)$:

$$\mathcal{E}_1 = E_D + \mathcal{E}_1^{(2)}\delta^2 + o(\delta^2), \quad \mathcal{E}_2 = E_D + \mathcal{E}_2^{(2)}\delta^2 + o(\delta^2), \quad (5.2)$$

where $\mathcal{E}_1^{(2)} \neq \mathcal{E}_2^{(2)}$;

2. $\psi_1(\mathbf{x})$ and $\psi_2(\mathbf{x})$ are well-approximated by two slow modulations of linear combinations of a basis of $\text{Ker}(\mathcal{H}_V - E_D)$:

$$\begin{aligned} \psi_1(\mathbf{x}) &= c_1^1 \sum_{j=1}^4 \alpha_j^1(\zeta) \phi_j(\mathbf{x}) + c_1^2 \sum_{j=1}^4 \alpha_j^2(\zeta) \phi_j(\mathbf{x}) + O_{H^2(\mathbb{R}^2/\mathbb{Z}\mathbf{w}_1)}(\delta^{\frac{1}{2}}), \\ \psi_2(\mathbf{x}) &= c_2^1 \sum_{j=1}^4 \alpha_j^1(\zeta) \phi_j(\mathbf{x}) + c_2^2 \sum_{j=1}^4 \alpha_j^2(\zeta) \phi_j(\mathbf{x}) + O_{H^2(\mathbb{R}^2/\mathbb{Z}\mathbf{w}_1)}(\delta^{\frac{1}{2}}), \end{aligned} \quad (5.3)$$

where $\{\phi_j(\mathbf{x})\}$ are the basis of $\text{Ker}(\mathcal{H}_V - E_D)$ as in the Theorem 2.4, $\zeta = \delta \mathbf{l}_2 \cdot \mathbf{x}$ is the slow variable, and $\alpha^l(\zeta)$ are two orthonormal topologically protected zero-energy eigenstates of Dirac operator $\mathcal{D}(0)$ in (4.17).

Remark 5.2 The second order non-degeneracy condition (5.1) guarantees $\mathcal{E}_1^{(2)} \neq \mathcal{E}_2^{(2)}$. The form of this condition changes with the phase transformation of $\phi_1(\mathbf{x})$, and therefore we fix a $\phi_1(\mathbf{x})$ which makes (3.9) valid.

This theorem states that $\mathcal{H}_{edge}^\delta$ has two gapped edge states at $k_{\parallel} = 0$ when δ is sufficiently small and characterizes the two edge modes by degenerate eigenmodes of \mathcal{H}_V . Before giving the comprehensive proof, we show some numerical results in Figure 3 that explicitly illustrate the conclusions. Figure (a) and (b) are the two gapped edge states at $k_{\parallel} = 0$ near the edge. Figure (c)-(f) are a basis of the four-dimensional eigenspaces of the unperturbed bulk operator with eigenvalue E_D . We choose a particular basis of the four-dimensional eigenspaces such that the eigenstates in figure (a) and figure (b) are modulations of the eigenstates in figure (c) and figure (d) respectively.

From the last section, we can obtain formal expansions of the two edge states at $k_{\parallel} = 0$:

$$\mathcal{E}_1(\delta) = E_D + \delta^2 \mu_1, \quad \psi_1(\mathbf{x}, \zeta; \delta) = \psi_1^{(0)}(\mathbf{x}, \zeta) + \delta \psi_1^{(1)}(\mathbf{x}, \zeta) + \delta g(\mathbf{x}); \quad (5.4)$$

$$\mathcal{E}_2(\delta) = E_D + \delta^2 \mu_2, \quad \psi_2(\mathbf{x}, \zeta; \delta) = \psi_2^{(0)}(\mathbf{x}, \zeta) + \delta \psi_2^{(1)}(\mathbf{x}, \zeta) + \delta h(\mathbf{x}); \quad (5.5)$$

where the $O(1)$ and $O(\delta)$ terms are as in the last subsection:

$$\begin{aligned} \psi_1^{(0)}(\mathbf{x}, \zeta) &= c_1^1 \Phi(\mathbf{x})^T \alpha^1(\zeta) + c_1^2 \Phi(\mathbf{x})^T \alpha^2(\zeta), \\ \psi_1^{(1)}(\mathbf{x}, \zeta) &= \Phi(\mathbf{x})^T \beta_1(\zeta; 0) + (\mathcal{H}_V - E_D)^{-1} \mathcal{L}_1(s) \psi_1^{(0)}(\mathbf{x}, \zeta); \end{aligned} \quad (5.6)$$

$$\begin{aligned} \psi_2^{(0)}(\mathbf{x}, \zeta) &= c_2^1 \Phi(\mathbf{x})^T \alpha^1(\zeta) + c_2^2 \Phi(\mathbf{x})^T \alpha^2(\zeta), \\ \psi_2^{(1)}(\mathbf{x}, \zeta) &= \Phi(\mathbf{x})^T \beta_2(\zeta; 0) + (\mathcal{H}_V - E_D)^{-1} \mathcal{L}_1(s) \psi_2^{(0)}(\mathbf{x}, \zeta). \end{aligned} \quad (5.7)$$

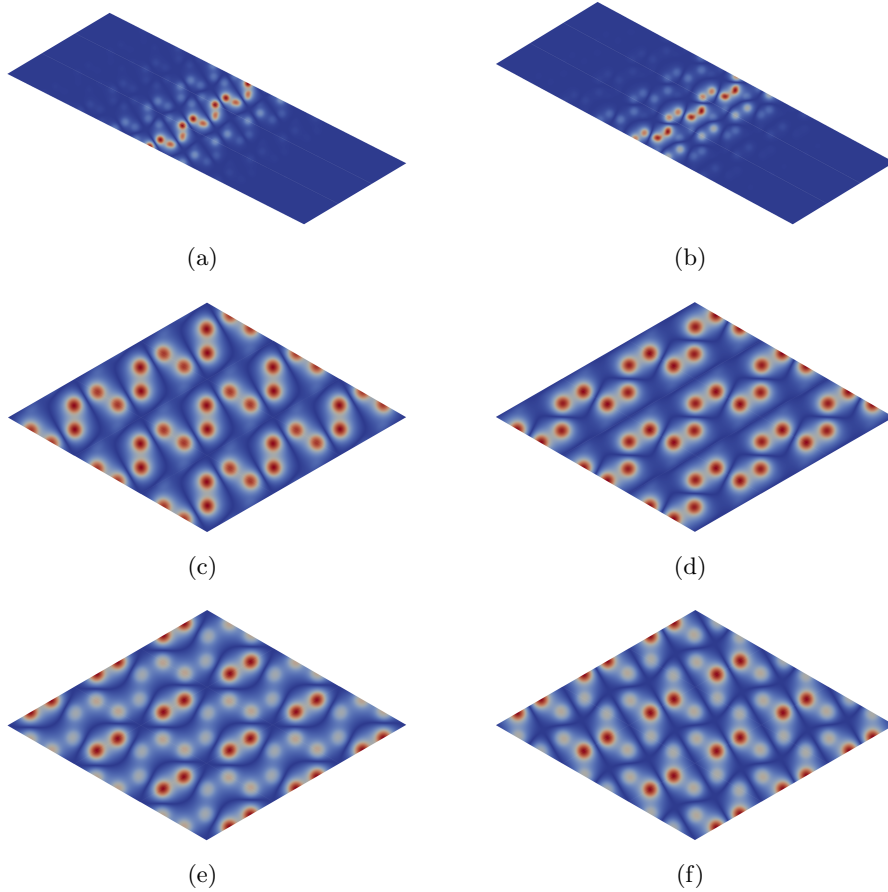


Figure 3: Figures of edge and bulk modes. (a) and (b) the figures of numerical solutions of two edge states at $k_{\parallel} = 0$ of the limiting domain wall model in Figure 1. (c), (d), (e), and (f) the figures of numerical solutions of fourfold degenerate bulk modes of corresponding unperturbed bulk operators. The eigenstates in figure (a) and figure (b) are modulations of the eigenstates in figure (c) and figure (d), respectively.

Substituting (5.4) into the eigenvalue problem at $k_{\parallel} = 0$, we can obtain the corrector equation:

$$\begin{aligned} & (\mathcal{H}_V - E_D)g(\mathbf{x}) + \delta\eta(\delta\mathbf{l}_2 \cdot \mathbf{x})W(\mathbf{x})g(\mathbf{x}) - \delta^2\mu_1g(\mathbf{x}) \\ &= \delta(\|\mathbf{l}_2\|^2\partial_{\zeta}^2 + \mu_1)\psi^{(0)}(\mathbf{x}, \zeta)|_{\zeta=\delta\mathbf{l}_2 \cdot \mathbf{x}} + \delta^2(\|\mathbf{l}_2\|^2\partial_{\zeta}^2 + \mu_1)\psi^{(1)}(\mathbf{x}, \zeta)|_{\zeta=\delta\mathbf{l}_2 \cdot \mathbf{x}} \\ &+ \delta(2\mathbf{l}_2 \cdot \nabla_{\mathbf{x}}\partial_{\zeta} - \eta(\zeta)W(\mathbf{x}))\psi^{(1)}(\mathbf{x}, \zeta)|_{\zeta=\delta\mathbf{l}_2 \cdot \mathbf{x}} \quad , \end{aligned} \quad (5.8)$$

and the same equation for μ_2 and $h(\mathbf{x})$. It remains to solve this equation and estimate the order of $g(\mathbf{x})$. We only need to construct rigorous results for (5.8), and the same can be done for μ_2 and $h(\mathbf{x})$. The idea is to decompose $g(\mathbf{x})$ by Floquet-Bloch modes and decompose the equation into different components accordingly [13]. Far-energy components can be solved as a functional of near-energy components. See section 3.2 for the description of near-energy approximation. Finally, we get a closed system of near-energy components, where we can use Lyapunov-Schmidt reduction.

It is obvious that $g(\mathbf{x})$ should be in χ_e . The following lemma shows that Floquet-Bloch eigenmodes are a complete basis for χ_e . According to this lemma, equation (5.8) can be decomposed into a family of equations.

Lemma 5.3 *For $f \in \chi_e$, where χ_e is defined in (4.2), the following decomposition is true:*

$$f(\mathbf{x}) = \sum_{n \geq 1} \int_{-\frac{1}{2}}^{\frac{1}{2}} \tilde{f}_n(\lambda) e_n(\mathbf{x}; \lambda \mathbf{l}_2) d\lambda. \quad (5.9)$$

Here $\{e_n(\mathbf{x}; \mathbf{k})\}_{n \in \mathbb{N}^*}$ are a complete orthonormal basis of $L_{\mathbf{k}}^2(\mathbb{R}^2/\mathbf{U})$ given by normaralized eigenstates of \mathcal{H}_V on $L_{\mathbf{k}}^2(\mathbb{R}^2/\mathbf{U})$. They are called Floquet-Bloch modes. And

$$\tilde{f}_n(\lambda) = \langle f(\mathbf{x}), e_n(\mathbf{x}; \lambda \mathbf{l}_2) \rangle_{L^2(\Omega_e)}. \quad (5.10)$$

For eigenmodes $e_n(\mathbf{x}; \lambda \mathbf{l}_2)$ with eigenvalue near E_D , there exists near energy approximations; see Proposition 3.6. We rearrange the spectrum and complete orthonormal eigenmodes accordingly:

$$\begin{aligned} E_n(\lambda) &= \begin{cases} \theta_j(\lambda), & n = n_* + j, \quad j = 1, 2, 3, 4, \quad |\lambda| \leq \delta^\nu \\ E_n(\lambda \mathbf{l}_2), & \text{else;} \end{cases} \\ e_n(\mathbf{x}; \lambda) &= \begin{cases} \Theta_j(\mathbf{x}; \lambda), & n = n_* + j, \quad j = 1, 2, 3, 4, \quad |\lambda| \leq \delta^\nu \\ e_n(\mathbf{x}; \lambda \mathbf{l}_2), & \text{else.} \end{cases} \end{aligned}$$

Now let us take inner products of (5.8) with $e_n(\mathbf{x}; \lambda)$ to obtain equations of $\{\tilde{g}_n(\lambda)\}_n$:

$$\begin{aligned} & (E_n(\lambda) - E_D)\tilde{g}_n(\lambda) + \delta\langle e_n(\cdot; \lambda), \eta(\delta\mathbf{l}_2 \cdot)W(\cdot)g(\cdot) \rangle_{L^2(\Omega_e)} \\ &= \delta F_n(\lambda; \delta, \mu_1) + \delta^2\mu_1\tilde{g}_n(\lambda). \end{aligned} \quad (5.11)$$

Here

$$\begin{aligned} F_n(\lambda; \delta, \mu_1) &= F_n^1(\lambda; \delta, \mu_1) + F_n^2(\lambda; \delta, \mu_1) + \delta F_n^3(\lambda; \delta, \mu_1), \\ F_n^1(\lambda; \delta, \mu_1) &= \langle e_n(\mathbf{x}; \lambda), (\|\mathbf{l}_2\|^2\partial_{\zeta}^2 + \mu_1)\psi^{(0)}(\mathbf{x}, \zeta)|_{\zeta=\delta\mathbf{l}_2 \cdot \mathbf{x}} \rangle_{L^2(\Omega_e)}, \\ F_n^2(\lambda; \delta, \mu_1) &= \langle e_n(\mathbf{x}; \lambda), (2\mathbf{l}_2 \cdot \nabla_{\mathbf{x}}\partial_{\zeta} - \eta(\zeta)W(\mathbf{x}))\psi^{(1)}(\mathbf{x}, \zeta)|_{\zeta=\delta\mathbf{l}_2 \cdot \mathbf{x}} \rangle_{L^2(\Omega_e)}, \\ F_n^3(\lambda; \delta, \mu_1) &= \langle e_n(\mathbf{x}; \lambda), (\|\mathbf{l}_2\|^2\partial_{\zeta}^2 + \mu_1)\psi^{(1)}(\mathbf{x}, \zeta)|_{\zeta=\delta\mathbf{l}_2 \cdot \mathbf{x}} \rangle_{L^2(\Omega_e)}. \end{aligned}$$

$\tilde{g}_n(\lambda)$ can be decomposed into several parts $\tilde{g}_n(\lambda) = \sum_{j=1}^4 \tilde{g}_{j,near}(\lambda) + \tilde{g}_{n,far}(\lambda)$:

$$\tilde{g}_{j,near}(\lambda) = \chi_{near}(\delta) \tilde{g}_{n_*+j}(\lambda), \quad (5.12)$$

$$\tilde{g}_{n,far}(\lambda) = \chi_{n,far}(\delta) \tilde{g}_n(\lambda). \quad (5.13)$$

Here

$$\chi_{near}(\delta) = \chi(|\lambda| \leq \delta^\nu), \quad \chi_{n,far}(\delta) = \chi\left(\left(\sum_{j=1}^4 \delta_{n,n_*+j}\right) \delta^\nu \leq \lambda \leq \frac{1}{2}\right),$$

ν is chosen appropriately by spectral no-fold condition (2.12) [11, 13] and δ_{n,n_*+j} are Kronecker delta symbols. Accordingly we obtain $g(\mathbf{x}) = g_{near}(\mathbf{x}) + g_{far}(\mathbf{x})$:

$$g_{near}(\mathbf{x}) = \sum_{j=1}^4 \int_{-\frac{1}{2}}^{\frac{1}{2}} \tilde{g}_{j,near}(\lambda) \Theta_j(\mathbf{x}; \lambda) d\lambda, \quad (5.14)$$

$$g_{far}(\mathbf{x}) = \sum_{n \geq 1} \int_{-\frac{1}{2}}^{\frac{1}{2}} \tilde{g}_{n,far}(\lambda) e_n(\mathbf{x}; \lambda) d\lambda. \quad (5.15)$$

Therefore, we can divide equations (5.11) into near energy components:

$$\begin{aligned} & (\theta_j(\lambda) - E_D) \tilde{g}_{j,near}(\lambda) \\ & + \delta \chi_{near}(\delta) \langle \Theta_j(\cdot; \lambda), \eta(\delta \mathbf{l}_2 \cdot) W(\cdot) (g_{near}(\cdot) + g_{far}(\cdot)) \rangle_{L^2(\Omega_e)} \\ & = \chi_{near}(\delta) \delta F_{n_*+j}(\lambda; \delta, \mu_1) + \delta^2 \mu_1 \tilde{g}_{j,near}(\lambda); \end{aligned} \quad (5.16)$$

and far energy components:

$$\begin{aligned} & (E_n(\lambda) - E_D) \tilde{g}_{n,far}(\lambda) \\ & + \delta \chi_{n,far}(\delta) \langle e_n(\cdot; \lambda), \eta(\delta \mathbf{l}_2 \cdot) W(\cdot) (g_{near}(\cdot) + g_{far}(\cdot)) \rangle_{L^2(\Omega_e)} \\ & = \chi_{n,far}(\delta) \delta F_n(\lambda; \delta, \mu_1) + \delta^2 \mu_1 \tilde{g}_{n,far}(\lambda). \end{aligned} \quad (5.17)$$

Rewrite the equation of far-energy components (5.17) as:

$$\begin{aligned} & -\delta \frac{\chi_{n,far}(\delta)}{E_n(\lambda) - E_D} \langle e_n(\cdot; \lambda), \eta(\delta \mathbf{l}_2 \cdot) W(\cdot) (g_{near}(\mathbf{x}) + g_{far}(\cdot)) \rangle_{L^2(\Omega_e)} \\ & + \delta \frac{\chi_{n,far}(\delta)}{E_n(\lambda) - E_D} F_n(\lambda; \delta, \mu_1) + \delta^2 \frac{\mu_1 \tilde{g}_{n,far}(\lambda)}{E_n(\lambda) - E_D} = \tilde{g}_{n,far}(\lambda). \end{aligned}$$

This can be viewed as a fixed problem of $\{\tilde{g}_{n,far}(\lambda)\}$ and easily transformed into a fixed point problem of $g_{far}(\mathbf{x})$ by (5.15). Fixing δ and μ_1 , via contraction mapping principle, $g_{far}(\mathbf{x})$ can be solved out as a functional of $g_{near}(\mathbf{x})$: $g_{far}(\mathbf{x}) = g_{far}[g_{near}; \mu_1, \delta](\mathbf{x})$.

Now let us look at (5.16) – the equation of near-energy components. Substituting $g_{far}(\mathbf{x}) = g_{far}[g_{near}; \mu_1, \delta](\mathbf{x})$ into (5.16), using the rescaling $\xi = \frac{\lambda}{\delta}$ and the results in Proposition 3.6 and canceling a factor of δ , we can finally obtain the closed system of near-energy components:

$$\begin{aligned} & -v_F \|\mathbf{l}_2\| \xi \tilde{g}_{j,near}(\delta \xi) + \chi_{near}(\delta) \langle \Theta_j(\cdot; \delta \xi), \eta(\mathbf{l}_2 \cdot) W(\cdot) g_{near}(\cdot) \rangle_{L^2(\Omega_e)} \\ & = \chi_{near}(\delta) F_{b+j}(\delta \xi; \delta, \mu_1) - \delta r_j(\delta \xi) \xi^2 \tilde{g}_{j,near}(\lambda) + \delta \mu_1 \tilde{g}_{j,near}(\delta \xi) \\ & - \chi_{near}(\delta) \langle \Theta_j(\cdot; \delta \xi), \eta(\mathbf{l}_2 \cdot) W(\cdot) g_{far}[g_{near}; \mu_1, \delta](\cdot) \rangle_{L^2(\Omega_e)}. \end{aligned} \quad (5.18)$$

The rest of the steps are transforming this system into a Dirac system, solving the system by Lyapunov-Schmidt reduction, and obtaining upper bound estimations of μ_1 and $g(\mathbf{x})$, which is similar to the \mathcal{PT} symmetry breaking case [13].

6 Physical interpretations

6.1 A topological view – parities

The differences between perturbed bulk operators $\mathcal{H}_{\pm}^{\delta}$ can be explained by the parities of eigenstates. Such parities originate in the C_6 symmetry and the time-reversal symmetry. We call them “topological” because they are stable against a family of small perturbations.

For δ sufficiently small, let us begin with the first-order bifurcation matrix of \mathcal{H}^{δ} [8]:

$$B_1^{\delta}(\mathbf{k}) = \begin{pmatrix} 0 & 2i\mathbf{k} \cdot \mathbf{v}_{\#} & -\delta c_{\#} & 0 \\ \overline{2i\mathbf{k} \cdot \mathbf{v}_{\#}} & 0 & 0 & -\delta c_{\#} \\ -\delta c_{\#} & 0 & 0 & -2i\mathbf{k} \cdot \mathbf{v}_{\#} \\ 0 & -\delta c_{\#} & \overline{-2i\mathbf{k} \cdot \mathbf{v}_{\#}} & 0 \end{pmatrix}. \quad (6.1)$$

Solve $(\lambda(\mathbf{k}; \delta)I + B_1^{\delta}(\mathbf{k}))\mathbf{P}(\mathbf{k}; \delta) = 0$ and obtain $\lambda_{\pm}(\mathbf{k}; \delta) = \pm\sqrt{4\|\mathbf{k} \cdot \mathbf{v}_{\#}\|^2 + \delta^2 c_{\#}^2}$. Both $\lambda_{\pm}(\mathbf{k}; \delta)$ are of multiplicity two. The corresponding eigenvectors are:

$$\mathbf{P}_{\pm,1}(\mathbf{k}; \delta) = \frac{1}{\sqrt{2}\lambda_{\pm}} \begin{pmatrix} \lambda_{\pm} \\ \overline{2i\mathbf{k} \cdot \mathbf{v}_{\#}} \\ -\delta c_{\#} \\ 0 \end{pmatrix}; \quad \mathbf{P}_{\pm,2}(\mathbf{k}; \delta) = \frac{1}{\sqrt{2}\lambda_{\pm}} \begin{pmatrix} 0 \\ -\delta c_{\#} \\ -2i\mathbf{k} \cdot \mathbf{v}_{\#} \\ \lambda_{\pm} \end{pmatrix}.$$

When $\mathbf{k} = 0$, we obtain that:

$$\mathbf{P}_{\pm,1}(\mathbf{0}; \delta) = \frac{1}{\sqrt{2}} \begin{pmatrix} 1 \\ 0 \\ \mp \text{sgn}(\delta c_{\#}) \\ 0 \end{pmatrix}; \quad \mathbf{P}_{\pm,2}(\mathbf{0}; \delta) = \frac{1}{\sqrt{2}} \begin{pmatrix} 0 \\ \mp \text{sgn}(\delta c_{\#}) \\ 0 \\ 1 \end{pmatrix}.$$

This means the main terms of the corresponding eigenstates are:

$$\begin{aligned} \phi_{\pm,1}(\mathbf{x}; \delta) &= \frac{1}{\sqrt{2}} (\phi_1(\mathbf{x}) \mp \text{sgn}(\delta c_{\#}) \phi_3(\mathbf{x})); \\ \phi_{\pm,2}(\mathbf{x}; \delta) &= \frac{1}{\sqrt{2}} (\phi_4(\mathbf{x}) \mp \text{sgn}(\delta c_{\#}) \phi_2(\mathbf{x})). \end{aligned}$$

The first interesting observation is that $\phi_{\pm,2}(\mathbf{x}) = \mathcal{T}[\phi_{\pm,1}](\mathbf{x})$, which means that these two states are connected by time-reversal symmetry.

Besides, note that $\phi_3(\mathbf{x}) = \phi_1(-\mathbf{x})$ and $\phi_2(\mathbf{x}) = \phi_4(-\mathbf{x})$. Thus, $\phi_{+,1}(\mathbf{x})$ and $\phi_{+,2}(\mathbf{x})$ are even when $\text{sgn}(\delta c_{\#}) = -1$, and are odd when $\text{sgn}(\delta c_{\#}) = 1$. The parity of $\phi_{-,1}(\mathbf{x})$ and $\phi_{-,2}(\mathbf{x})$ are opposite to them. This means that the parities of the upper two bands at the Γ point

are always the same and opposite to those of the lower two bands. And the parities change when $\text{sgn}(\delta c_{\sharp})$ changes.

These observations are true for not only the main terms but also the true eigenstates at the Γ point when adding small folding symmetry breaking perturbations. This result originates in the C_6 symmetry and \mathcal{PT} symmetry of the operator \mathcal{H}^δ and the C_6 symmetry of the Γ point:

$$\chi = \bigoplus_{l=0}^5 \tilde{\chi}_l; \quad \tilde{\chi}_l = \{f \in \chi : \tilde{\mathcal{R}}[f](\mathbf{x}) = e^{\frac{\pi i}{3}l} f(\mathbf{x})\}. \quad (6.2)$$

$\tilde{\mathcal{R}}$ is the $\frac{\pi}{3}$ -rotation operator: $\tilde{\mathcal{R}}[f](\mathbf{x}) = f(\tilde{R}^* \mathbf{x})$, where

$$\tilde{R}^* = \begin{pmatrix} \frac{1}{2} & \frac{\sqrt{3}}{2} \\ -\frac{\sqrt{3}}{2} & \frac{1}{2} \end{pmatrix}$$

represents the anticlock $\frac{\pi}{3}$ -rotation in \mathbb{R}^2 . \mathcal{H}^δ is commutative with $\tilde{\mathcal{R}}$. Thus, each $\tilde{\chi}_l$ is an invariant subspace of \mathcal{H}^δ . These characteristic subspaces of $\tilde{\mathcal{R}}$ have the following properties associated with \mathcal{P} and \mathcal{T} symmetries.

- Each $\tilde{\chi}_l$ is \mathcal{P} invariant: because $\mathcal{P} = \tilde{\mathcal{R}} \circ \tilde{\mathcal{R}} \circ \tilde{\mathcal{R}}$, any $f(\mathbf{x})$ in $\tilde{\chi}_l$ is even when j is even and odd when j is odd.
- $\tilde{\chi}_l$ and $\tilde{\chi}_{6-l}$ are reflected to each other by \mathcal{T} : if $f(\mathbf{x})$ is in $\tilde{\chi}_l$, then $\mathcal{T}[f](\mathbf{x})$ is in $\tilde{\chi}_{6-l}$; specially if $f(\mathbf{x})$ is in $\tilde{\chi}_0$, then $\mathcal{T}[f](\mathbf{x})$ is in $\tilde{\chi}_0$, too.

The eigenstates $\phi_l(\mathbf{x})$ of $H^0 = \mathcal{H}_V$ are in characteristic subspaces of \mathcal{R} and \mathcal{V}_1 as in the second conclusion in Theorem 2.4. After some linear combinations, they can be rearranged into:

$$\begin{aligned} \tilde{\phi}_1(\mathbf{x}) &= \frac{1}{\sqrt{2}}(\phi_1(\mathbf{x}) + \phi_3(\mathbf{x})) \in \tilde{\chi}_4; \\ \tilde{\phi}_2(\mathbf{x}) &= \frac{1}{\sqrt{2}}(\phi_4(\mathbf{x}) + \phi_2(\mathbf{x})) \in \tilde{\chi}_2; \\ \tilde{\phi}_3(\mathbf{x}) &= \frac{1}{\sqrt{2}}(\phi_1(\mathbf{x}) - \phi_3(\mathbf{x})) \in \tilde{\chi}_1; \\ \tilde{\phi}_4(\mathbf{x}) &= \frac{1}{\sqrt{2}}(\phi_4(\mathbf{x}) - \phi_2(\mathbf{x})) \in \tilde{\chi}_5. \end{aligned}$$

By the continuity of the spectrum concerning δ [12], the four branches $\{E_{b+j}(\mathbf{k}; \delta) : \mathbf{k} \in \Omega^*\}_{j=1,2,3,4}$ possess eigenstates in $\tilde{\chi}_1, \tilde{\chi}_2, \tilde{\chi}_4, \tilde{\chi}_5$ respectively and decompose into a pair of twofold degeneracy since $\tilde{\chi}_l$ and $\tilde{\chi}_{6-l}$ are connected by \mathcal{T} symmetry. This confirms that the upper or lower two bands have the same parity.

6.2 Second-order bifurcations and the \mathcal{PT} symmetry preserving

It is necessary to calculate second-order terms in the near-energy approximation and edge states problems because they both have degeneracy at the first order. Only through the higher-order terms can we know one simple eigenvalue crystal clear when it gets entangled

with another one at lower orders. The mechanism behind this behavior originates in the property of \mathcal{PT} symmetry preserving.

For the single Dirac cone case, the bifurcation matrix is a 2×2 matrix, and we can associate the topology of the perturbed bulk operator \mathcal{H}^δ with the topology of the effective two-band model given by the first-order bifurcation matrix [9, 10]. This works because the first-order bifurcation matrix in the single Dirac cone case has two simple eigenvalues and two separated bundles of eigenvectors. However, for the double Dirac cone, this is not true because the eigenvalues are of multiplicity two. Only by adding higher-order terms can we correctly separate the eigenvalues into four simple eigenvalues.

Still, recall the first-order bifurcation matrix $B_1^\delta(\mathbf{k})$ of \mathcal{H}^δ in (6.1). This matrix can be transformed by Q mentioned in (4.13) into:

$$\begin{aligned} \tilde{B}_1^\delta(\mathbf{k}) &= Q^T B_1^\delta(\mathbf{k}) Q = \begin{pmatrix} -\delta c_\sharp & 2i\mathbf{k} \cdot \mathbf{v}_\sharp & 0 & 0 \\ \frac{2i\mathbf{k} \cdot \mathbf{v}_\sharp}{\delta c_\sharp} & \delta c_\sharp & 0 & 0 \\ 0 & 0 & \delta c_\sharp & 2i\mathbf{k} \cdot \mathbf{v}_\sharp \\ 0 & 0 & \frac{2i\mathbf{k} \cdot \mathbf{v}_\sharp}{\delta c_\sharp} & -\delta c_\sharp \end{pmatrix} \\ &= \text{diag}(B_s(\mathbf{k}; \delta), B_s(\mathbf{k}; -\delta)). \end{aligned}$$

Here

$$B_s(\mathbf{k}; \delta) = \begin{pmatrix} -\delta c_\sharp & 2i\mathbf{k} \cdot \mathbf{v}_\sharp \\ \frac{2i\mathbf{k} \cdot \mathbf{v}_\sharp}{\delta c_\sharp} & \delta c_\sharp \end{pmatrix}$$

is the first-order bifurcation matrix for the perturbed single Dirac cone, where the \mathcal{PT} symmetry is broken [11]. From diagonal elements, $\tilde{B}_1^\delta(\mathbf{k})$ looks like a superposition of two perturbed single Dirac cones. But take care of the fact that although they can be decoupled in the form, they are actually coupled because they have the same eigenvalues. Intrinsically, such coupling roots in the \mathcal{PT} symmetry preserving property. If we want to characterize the topology of each energy band, we have to separate the bands by some methods, such as considering the higher-order terms, from which we can also make it clear how they are coupled.

The determining part of the next-order bifurcation matrix, after some calculation, is

$$\tilde{B}_2^\delta(\mathbf{k}) = Q^T B_2^\delta(\mathbf{k}) Q = \begin{pmatrix} 0 & 0 & 0 & b(\mathbf{k}) \\ 0 & 0 & \overline{b(\mathbf{k})} & 0 \\ 0 & b(\mathbf{k}) & 0 & 0 \\ \overline{b(\mathbf{k})} & 0 & 0 & 0 \end{pmatrix}.$$

Here $b(\mathbf{k})$ is the second-order term as in (3.6):

$$b(\mathbf{k}) = \langle \phi_1(\mathbf{x}), 2i\mathbf{k} \cdot \nabla(\mathcal{H}_V - E_D)^{-1} \mathcal{Q}_\perp 2i\mathbf{k} \cdot \nabla \overline{\phi_1(-\mathbf{x})} \rangle_{L^2(\Omega)}.$$

Take the two bands with eigenvalues whose leading terms are $\lambda_+(\mathbf{k}; \delta) = \sqrt{4\|\mathbf{k} \cdot \mathbf{v}_\sharp\|^2 + \delta^2 c_\sharp^2}$ as examples. By Lyapunov-Schmidt reduction, the associated leading terms of eigenvectors are:

$$\frac{|a_+(\mathbf{k}; \delta)|}{\sqrt{2}|a_+(\mathbf{k}; \delta)|} \begin{pmatrix} \delta c_\sharp - \lambda_+ \\ -2i\mathbf{k} \cdot \mathbf{v}_\sharp \\ 0 \\ 0 \end{pmatrix} + \frac{\overline{a_+(\mathbf{k}; \delta)}}{\sqrt{2}|a_+(\mathbf{k}; \delta)|} \begin{pmatrix} 0 \\ 0 \\ -2i\mathbf{k} \cdot \mathbf{v}_\sharp \\ \delta c_\sharp - \lambda_+ \end{pmatrix},$$

and

$$\frac{a_+(\mathbf{k}; \delta)}{\sqrt{2}|a_+(\mathbf{k}; \delta)|} \begin{pmatrix} \delta c_{\#} - \lambda_+ \\ -2i\mathbf{k} \cdot \mathbf{v}_{\#} \\ 0 \\ 0 \end{pmatrix} - \frac{|a_+(\mathbf{k}; \delta)|}{\sqrt{2}|a_+(\mathbf{k}; \delta)|} \begin{pmatrix} 0 \\ 0 \\ -2i\mathbf{k} \cdot \mathbf{v}_{\#} \\ \delta c_{\#} - \lambda_+ \end{pmatrix}.$$

Here $a_+(\mathbf{k}; \delta)$ is such a quantity:

$$a_+(\mathbf{k}; \delta) = \frac{(2i\mathbf{k} \cdot \mathbf{v}_{\#})^2 \overline{b(\mathbf{k})} + (\delta c_{\#} - \lambda_+)^2 b(\mathbf{k})}{2\lambda_+(\lambda_+ - \delta c_{\#})}.$$

This shows the second-order terms influence the properties of the energy bands no less than the first-order terms.

Besides, let us consider the grading operator G :

$$G = \begin{pmatrix} 0 & 0 & 0 & 1 \\ 0 & 0 & -1 & 0 \\ 0 & 1 & 0 & 0 \\ -1 & 0 & 0 & 0 \end{pmatrix}$$

satisfying $G^2 = -I$. The bifurcation matrices satisfy:

$$G^* \tilde{B}_1^\delta(\mathbf{k}) G = \overline{\tilde{B}_1^\delta(\mathbf{k})}; \quad G^* \tilde{B}_2^\delta(\mathbf{k}) G = -\overline{\tilde{B}_2^\delta(\mathbf{k})}.$$

Such difference between $\tilde{B}_1^\delta(\mathbf{k})$ and $\tilde{B}_2^\delta(\mathbf{k})$ indicates that the first order approximation is more ‘‘symmetric’’ than the original problem and results in the gap between two edge states [6].

6.3 A typical example

A typical example in physics is the kind of \mathcal{PT} symmetric structure proposed by Wu and Hu [29]. We numerically study the associated edge Schrödinger operator:

$$\mathcal{H}_{edge} = -\Delta + W_{edge}(\mathbf{x}).$$

Here the potential $W_{edge}(\mathbf{x})$ is a piecewise constant function in $L^2(\mathbb{R}^2)$. In the analysis in the above sections, we always suppose all the potentials are smooth. For general discontinuous potentials in $L^2(\mathbb{R}^2)$, Theorem 2.6, Theorem 3.4, and the multiscale expansions are still valid, but other results should be treated carefully after smoothing, especially for the error estimation.

The parameters related to the honeycomb lattice are:

$$\mathbf{u}_1 = \begin{pmatrix} \frac{\sqrt{3}}{2} \\ \frac{1}{2} \end{pmatrix}, \quad \mathbf{u}_2 = \begin{pmatrix} \frac{\sqrt{3}}{2} \\ -\frac{1}{2} \end{pmatrix}, \quad \mathbf{u}_3 = \mathbf{u}_2 - \mathbf{u}_1 = \begin{pmatrix} 0 \\ -1 \end{pmatrix};$$

$$\mathbf{k}_1 = \frac{4\pi}{\sqrt{3}} \begin{pmatrix} \frac{1}{2} \\ \frac{\sqrt{3}}{2} \end{pmatrix}, \quad \mathbf{k}_2 = \frac{4\pi}{\sqrt{3}} \begin{pmatrix} \frac{1}{2} \\ -\frac{\sqrt{3}}{2} \end{pmatrix}.$$

The edge direction is $\boldsymbol{l}_2 = \mathbf{k}_2$. The potential is

$$W_{edge}(\mathbf{x}) = \begin{cases} g(\mathbf{x}; \frac{1.1}{3}), & \mathbf{x} \cdot \boldsymbol{l}_2 \geq 0; \\ g(\mathbf{x}; \frac{0.9}{3}), & \text{else.} \end{cases}$$

Here $g(\mathbf{x}, \frac{1.1}{3})$ and $g(\mathbf{x}, \frac{0.9}{3})$ are the perturbed bulk potentials on the two sides of the edge with different topologies. They are deformed from $g(\mathbf{x}; \frac{1}{3})$ – a potential possessing all the properties of the super honeycomb lattice potential except for the smoothness. They are shrunk and expanded super honeycomb lattice potentials respectively, as shown in Figure 1. They can be constructed by rotation of dimers as below:

$$g(\mathbf{x}; r) = f(\mathbf{x}; r) + \mathcal{R}f(\mathbf{x}; r) + \mathcal{R}^2f(\mathbf{x}; r).$$

The potential of a group of dimers is:

$$f(\mathbf{x}; r) = a(\mathbf{x} - \frac{1}{2}r\mathbf{u}_3) + a(\mathbf{x} + \frac{1}{2}r\mathbf{u}_3)$$

with $a(\mathbf{x})$ \mathbf{u}_1 and \mathbf{u}_2 doubly periodic. In the unit cell, it is

$$a(\mathbf{x}) = \begin{cases} 10, & |x - \frac{1}{2}(\mathbf{u}_1 + \mathbf{u}_2)| < 0.1, \\ 300, & \text{else.} \end{cases}$$

We use the finite element method [17] to get the picture of \mathcal{H}_{edge} 's spectrum and eigenstates as shown in Figure 1 and Figure 3. (b) of Figure 1 shows the existence of two gapped edge states. (a) and (b) of Figure 3 are corresponding eigenstates. (c)-(f) of Figure 3 are a basis of eigenstates of the operator

$$\mathcal{H}_{bulk} = -\Delta + g(\mathbf{x}; \frac{1}{3})$$

with energy E_D marked in (b) of Figure 1. The operator \mathcal{H}_{bulk} has a fourfold degeneracy on its energy band at the Γ point as in Theorem 2.4 with eigenstates (c)-(f). The edge modes in (a) and (b) are modulations of (c) and (d) in Figure 3.

Acknowledgment

We would like to acknowledge Guochuan Thiang and Borui Miao for inspiring discussions and precious suggestions and Shuo Yang for providing help in establishing numerical simulations. This work was funded by the National Key R&D Program of China (grant 2021YFA0719200).

References

- [1] M. J. Ablowitz and Y. Zhu., Nonlinear waves in shallow honeycomb lattices, *SIAM J. Appl. Math.* **72**(1) (2012) 240–260.

- [2] H. Ammari and J. Cao., Unidirectional edge modes in time-modulated metamaterials, *Proc. R. Soc. A.* **478** (2022) 20220395.
- [3] H. Ammari, B. Davies and E. O. Hiltunen, Robust edge modes in dislocated systems of subwavelength resonators, *J. London Math. Soc.* **106(3)** (2022) 2075–2135.
- [4] G. Bal, Continuous bulk and interface description of topological insulators, *J. Math. Phys.* **60(8)** (2019), 081506.
- [5] G. Bal, J. G. Hoskins, and Z. Wang, Asymmetric transport computations in Dirac models of topological insulators, *J. Comput. Phys.* **487** (2023) 112151.
- [6] G. Bal, and Z. Wang, \mathbb{Z}^2 classification of FTR symmetric differential operators and obstruction to Anderson localization, *arXiv:2311.05872* (2023).
- [7] S. Barik, H. Miyake, W. DeGottardi, E. Waks, and M. Hafezi, Two-dimensionally confined topological edge states in photonic crystals, *New J. Phys.* **18(11)** (2016) 113013.
- [8] Y. Cao and Y. Zhu, Double Dirac cones in band structures of periodic Schrödinger operators, *Multiscale Model. Simul.* **21(3)** (2023) 1147–1169.
- [9] A. Drouot, The bulk-edge correspondence for continuous honeycomb lattices, *Comm. Partial Differential Equations* **44(12)** (2019) 1406–1430.
- [10] A. Drouot, C. L. Fefferman, and M. I. Weinstein, Defect modes for dislocated periodic media, *Comm. Math. Phys.* **377(3)** (2020) 1637–1680.
- [11] A. Drouot and M. I. Weinstein, Edge states and the valley Hall effect, *Adv. Math.* **368** (2020) 107142.
- [12] C. L. Fefferman, J. P. Lee-Thorp, and M. I. Weinstein, Topologically protected states in one-dimensional continuous systems and Dirac points, *Proc. Natl. Acad. Sci. USA.* **111(24)** (2014) 8759–8763.
- [13] C. L. Fefferman, J. P. Lee-Thorp, and M. I. Weinstein, Edge states in honeycomb structures, *Ann. PDE* **2(2)** (2016) 12.
- [14] C. L. Fefferman and M. I. Weinstein, Honeycomb lattice potentials and Dirac points, *J. Amer. Math. Soc.* **25(4)** (2012) 1169–1220.
- [15] H. Guo and X. Yang, Deep unfitted Nitsche method for elliptic interface problems, *Commun. Comput. Phys.* **31(4)** (2022) 1162–1179.
- [16] H. Guo, X. Yang, and Y. Zhu, Unfitted Nitsche’s method for computing wave modes in topological materials, *J. Sci. Comput.* **88(1)** (2021) 24.
- [17] H. Guo, M. Zhang, and Y. Zhu, ThreeFold Weyl Points for the Schrödinger Operator with Periodic Potentials, *Siam. J. Math. Anal.* **54(3)** (2022) 3654–3695.

- [18] M. Z. Hasan and C. L. Kane, Colloquium: Topological insulators, *Rev. Mod. Phys.* **82** (2010) 3045–3067.
- [19] P. Hu, P. Xie, and Y. Zhu, Traveling edge states in massive Dirac equations along slowly varying edges, *IMA J. Appl. Math.* **88(3)** (2023) 455–471.
- [20] A. B. Khanikave, S. H. Mousavi, W.-K. Tse, M. Kargarian, A. H. MacDonald, and G. Shvets, Photonic topological insulators, *Nat. Mater.* **12** (2013) 233.
- [21] J. P. Lee-Thorp, M. I. Weinstein, and Y. Zhu, Elliptic operators with honeycomb symmetry: Dirac points, edge states and applications to photonic graphene, *Arch. Ration. Mech. Anal.* **232(1)** (2019) 1–63.
- [22] B. Miao and Y. Zhu, Generalized honeycomb-structured materials in the subwavelength regime, *arXiv:2303.15719* (2023)
- [23] Y. Ogata, A \mathbb{Z}^2 -index of symmetry protected topological phases with time reversal symmetry for quantum spin chains, *Commun. Math. Phys.* **374** (2020) 705–734.
- [24] S. J. Palmer and V. Giannini, Berry bands and pseudo-spin of topological photonic phases, *Phys. Rev. Res.* **3** (2021) L022013.
- [25] M. S. Rudner, N. H. Lindner, E. Berg, and M. Levin, Anomalous edge states and the bulk-edge correspondence for periodically driven two-dimensional systems, *Phys. Rev. X.* **3(3)** (2013) 031005.
- [26] D. Smirnova, S. Kruk, D. Leykam, E. Melik-Gaykazyan, D. Choi, and Y. Kivshar, Third-harmonic generation in photonic topological metasurfaces, *Phys. Rev. Lett.* **123** (2019) 103901.
- [27] G. C. Thiang, Topological edge states of 1D chains and index theory , *J. Math. Phys.*, **64** (2023) 061901.
- [28] G. C. Thiang, and H. Zhang, Bulk-interface correspondences for one dimensional topological materials with inversion symmetry, *Proc. Math. Phys. Eng. Sci.*, **479** (2023) 20220675.
- [29] L. Wu and X. Hu, Scheme for achieving a topological photonic crystal by using dielectric material, *Phys. Rev. Lett.* **114** (2015) 223901.
- [30] Y. Yang, Y. Xu, T. Xu, H. Wang, J. Jiang, X. Hu, and Z. Hang, Visualization of a unidirectional electromagnetic waveguide using topological photonic crystals made of dielectric materials, *Phys. Rev. Lett.* **120** (2018) 217401.
- [31] S. Yves, R. Fleury, T. Berthelot, M. Fink, F. Lemoult, and G. Lerosey, Crystallinemetamaterials for topological properties at subwavelength scales, *Nat. Commun.* **8(1)** (2017) 16023.